

This is a postprint version of the following published document:

Morassi, A.; Fernández-Sáez, J.; Zaera, R.; Loya, J.A. (2017). Resonator-based detection in nanorods, *Mechanical Systems and Signal Processing*, v. 93, pp.: 645-660.

DOI: <https://doi.org/10.1016/j.ymssp.2017.02.019>

© 2017 Elsevier Ltd. All rights reserved.



This work is licensed under a [Creative Commons AttributionNonCommercialNoDerivatives 4.0 International License](https://creativecommons.org/licenses/by-nc-nd/4.0/)

# Resonator-based detection in nanorods

A. Morassi<sup>a</sup>, J. Fernández-Sáez<sup>b,\*</sup>, R. Zaera<sup>b</sup>, J.A. Loya<sup>b</sup>

<sup>a</sup>*Polytechnic Department of Engineering and Architecture, University of Udine, via  
Cotonificio 114, 33100 Udine, Italy*

<sup>b</sup>*Department of Continuum Mechanics and Structural Analysis, Universidad Carlos III  
de Madrid, Av. de la Universidad 30, 28911 Leganés, Madrid, Spain*

---

## Abstract

In this paper the axial vibrational behaviour of nanorods with an attached point-mass is studied, using the modified strain energy theory. The natural frequencies of the nanorod with the concentrated mass are obtained for different boundary conditions. The effects of the concentrated mass intensity, mass location, as well as the value of scale parameters have been analysed. For the case of small intensity of the concentrated mass, the natural frequencies of the nanorod can be estimated using a first order perturbative solution. These approximate results are compared with those corresponding to the exact solution. For this case, from the properties of the eigenvalue perturbative theory, the identification of single point mass in uniform nanorods (mass intensity and position) is addressed. The results obtained encourage the use of axial vibrations of nanorods as a very precise sensing technique.

## *Keywords:*

Strain gradient theory, nanorods, nanosensors, mass identification, inverse

---

\*Corresponding author. E-mail address: jose.fernandez@uc3m.es

problems.

---

## 1. Introduction

Nowadays, the scientific community interest is attracted by the use of nanostructures (carbon nanotubes, *CNTs*, graphene sheets, *GSs*, and nanowires) as nano-sensors. The reason is connected with the promising features regarding a wide range of applications such as gas detection, early disease detection, gene mutation detection, DNA sequencing. In this respect, several reviews have been recently published showing the different capabilities of the nanostructures [1, 2, 3]. According to Khanna [4], nano-sensors can be classified into six groups: mechanical, electrical, optical, magnetic, chemical, and thermal.

In this research we are interested in mechanical nanoresonator sensors and, in particular, in vibration based-methods as identification techniques. The sensing principle for this class of nanoresonators is based on the measurement of the variations of the resonant frequencies caused by (unknown) additional masses located on the initial system. **The conventional detection principle assumes that the mass perturbation, caused by attachments of foreign atoms or molecules, chemical/molecular adsorption, the presence of virus particles or protein-protein and protein-DNA interactions, can be described as Dirac-delta point masses,** having unknown intensities and locations, superimposed to the given mass density of the nanoresonator. We refer to [1] and [5] for more sophisticated mechanical models in which a simultaneous perturbation of the stiffness properties coupled with the mass increase is also

considered in the analysis. Our main goals in the present research are: (i) to derive a continuum mechanical model able to describe the axial vibration of a nanoresonator with a single additional point mass, and (ii) to develop a method for the identification of the point mass from minimal eigenfrequency data. In particular, we shall consider the inverse problem in which the added mass is *small* with respect to the total mass of the nanosensor.

It is well known that the size effects are significant regarding the mechanical behavior of the nanostructures which composes the nanoresonators. The large computational effort required for the Molecular Dynamics techniques (*MD*), see, among others, [6, 7, 8, 9], encourages the exploration of other possibilities, such as generalized continuum mechanics approaches given that classical continuum mechanics cannot predict the size effect, due to its scale-free character.

Among the generalized continuum theories, we cite here three main groups: Cosserat micropolar elasticity [10], the strain gradient elasticity of Mindlin [11, 12], and the nonlocal continuum mechanics initiated by Eringen and coworkers [13, 14], and formulated originally in integral form.

From the early integral nonlocal theory, Eringen [15] introduced a differential constitutive theory showing that, for a specific class of kernel functions, the non-local integral constitutive equation can be transformed into a differential form, much easier to manage than the integral model. From the pioneer work of Peddieson et al. [16], this differential version of the Eringen nonlocal model has been widely used to address the mechanical behaviour (static and dynamic) of nano-structures. The list of papers related with these applica-

tions is extremely long to be reported here. The interested reader can read the very recent review by Rafii-Tabar et al. [17].

Several authors used the Eringen elasticity theory to assess the vibrational behaviour of beams and rods with attached masses. Thus, Elthaer et al. [18], Murmu et al. [19], and Li et al. [20] applied this theory to obtain the shift of the natural frequency of bending vibrations of nanobeams carrying attached mass. Moreover, Murmu et al. [19] and Li et al. [20] provided identification formulas from the approximated expressions of the frequency shift. However, the cases studied in the above papers are rather specific and correspond to a nano-cantilever with a mass attached at the tip or a distributed mass through a certain length from the tip [19], while three configurations, corresponding to a cantilever beam with a mass attached at the tip, simply supported, and bi-clamped beams with the mass attached at the mid-section, are analysed in [20].

Regarding the use of the Eringen elasticity theory applied to *CNTs* with a single attached mass vibrating in axial direction, it is worth to note the work by Aydogdu and Filiz [21] who analyzed the frequencies of axially vibrating *CNTs* (clamped-clamped and clamped-free) with a single attached mass located at different positions.

Li et al. [22] studied the natural frequencies of an axially vibrating nanorod with an elastically restrained end by a nanospring (depending of the stiffness of the nanospring this end could be considered clamped or free), and with an attached mass at the other end considered free. In this analysis, the Love hypotheses are considered (i.e. the inertial effects of radial motion

have been taken into account).

Nevertheless, several authors have pointed out some inconsistencies arising from the Eringen differential model when it is applied to the static behavior of bars in tension [23], static bending behaviour of a Euler-Bernoulli beams [16, 24, 25, 26, 27] or flexural vibrations of a cantilever beam [28].

Recently, Fernández-Sáez et al. [29] and Romano et al. [30] give some new insights on the origin of these inconsistencies. Therefore, a more suitable approach to describe the mechanical behaviour of the nanostructures is needed.

The modified strain gradient elasticity theory was proposed by Lam et al. [31] based on previous developments by Mindlin [12] and Fleck and Hutchinson [32]. This approach needs new additional equilibrium equations to govern the behavior of higher-order stresses, and contain only three non-classical constants for isotropic linear elastic materials. Some papers can be cited to illustrate (the list is not exhaustive) the use of this theory to model the mechanical behaviour of 1D simple nanostructures (beams and rods). Thus, using this approach the static and dynamic bending behavior of Euler-Bernoulli beams [33] and Timoshenko beams has been studied [34]. Akgoz and Civalek [35, 36] obtained analytical solutions for the buckling problem of axially loaded nano-sized beams. The free torsional vibrations of microbars have been analyzed in [37, 38]. Akgoz and Civalek also studied the longitudinal vibrations of homogeneous [39] and nonhomogeneous (functionally graded material) [40] microbars using the simple rod theory, while Guven [41] analyzed the propagation of longitudinal stress waves based on

Love-Bishop hypothesis, i.e. considering the lateral deformation and the shear strain effects.

To our knowledge, there is no theoretical investigation on the axial vibrations of nanorods with attached concentrated mass when the modified strain gradient elasticity theory of Lam et al. [31] is used as constitutive model. This analysis is relevant regarding the nanosensor applications of this kind of structures.

Regarding the experimental determination of frequencies in axially vibrating nanorods, some papers can be found in the literature (see for instance, [42, 43, 44]). However, to the authors knowledge, no experimental works dealing with axially vibrating nanorods with attached masses have been published.

In this paper we analyze the axial vibrational behavior of a nanorod carrying a concentrated mass through its span and subjected to different boundary conditions. The mechanical behavior of the nanorod is modelled using the modified strain gradient theory proposed by Lam et al. [31]. The effects of the mass intensity, location as well as the value of scale parameter have been analyzed. For the case of small intensity of the concentrated mass, a first order perturbative technique is used to estimate the natural frequencies of the nanorod. The approximate results are compared with those corresponding to the exact solution. Basing on the explicit expression of the first-order eigenfrequency change induced by the point mass, we are able to formulate and solve the inverse problem consisting in the identification of the location and intensity of the point mass in a uniform nanorod from

minimal eigenfrequency data. In particular, for nanorods under a specified set of end conditions, the method gives closed-form expressions of both the location and the intensity of the point mass in terms of a suitable pair of eigenfrequencies of the nanorod.

The paper is organized as follows. The mechanical model of the nanorod under longitudinal free vibration with and without point mass is briefly recalled in Section 2. Section 3 is devoted to the illustration of the perturbation effects of the small added mass on the eigenvalues of the nanorod. The inverse problem of identifying the position and the intensity of the small point mass from eigenfrequency shifts is addressed in Section 4. Applications and results of numerical simulations, both of the direct and the inverse eigenvalue problem, are reported and commented in Section 5.

## 2. The mechanical model

### 2.1. Brief resume of the modified strain gradient theory

The modified strain gradient theory was presented by Lam et al. [31], who considered the following expression for the strain energy  $\mathcal{W}$  corresponding to a linear elastic isotropic material occupying a volume  $V$

$$\mathcal{W} = \int_V \left( \sigma_{ij} \varepsilon_{ij} + p_i \gamma_i + \tau_{ijk}^{(1)} \eta_{ijk}^{(1)} + m_{ij}^s \chi_{ij}^s \right) dv, \quad (1)$$

where the notational convention that repeated indices are implicitly summed from 1 to 3 has been adopted hereinafter. Classical and higher order stress

measures  $\sigma_{ij}$ ,  $p_i$ ,  $\tau_{ijk}^{(1)}$ ,  $m_{ij}^s$  are defined as [31]

$$\sigma_{ij} = \left( K - \frac{2G}{3} \right) \delta_{ij} \varepsilon_{mm} + 2G \varepsilon_{ij}, \quad (2)$$

$$p_i = 2Gl_0^2 \gamma_i, \quad (3)$$

$$\tau_{ijk}^{(1)} = 2Gl_1^2 \eta_{ijk}^{(1)}, \quad (4)$$

$$m_{ij}^s = 2Gl_2^2 \chi_{ij}^s, \quad (5)$$

where the strain tensor  $\varepsilon_{ij}$ , the dilatational gradient vector  $\gamma_i$ , the deviatoric stretch gradient tensor  $\eta_{ijk}^{(1)}$  and the symmetric rotation gradient tensor  $\chi_{ij}^s$  are given by

$$\varepsilon_{ik} = \frac{1}{2} (u_{i,j} + u_{j,i}), \quad (6)$$

$$\gamma_i = \varepsilon_{mm,i}, \quad (7)$$

$$\begin{aligned} \eta_{ijk}^{(1)} = & \frac{1}{3} (\varepsilon_{jk,i} + \varepsilon_{ki,j} + \varepsilon_{ij,k}) - \\ & - \frac{1}{15} [\delta_{ij} (\varepsilon_{mm,k} + 2\varepsilon_{mk,m}) + \delta_{jk} (\varepsilon_{mm,i} + 2\varepsilon_{mi,m}) + \delta_{ki} (\varepsilon_{mm,j} + 2\varepsilon_{mj,m})], \end{aligned} \quad (8)$$

$$\chi_{ij}^s = \frac{1}{2} (\theta_{i,j} + \theta_{j,i}). \quad (9)$$

Here,  $u_i$  is the  $i$ th cartesian component of the displacement vector,  $i = 1, 2, 3$ , and  $\theta_i$  is the rotation vector expressed as

$$\theta_i = \frac{1}{2} e_{ijk} u_{k,j}. \quad (10)$$

$\delta_{ij}$  is the Kronecker delta, and  $e_{ijk}$  is the permutation symbol.

Bulk modulus  $K = E/(3(1 - 2\nu))$ ,  $K > 0$ , and shear modulus  $G = E/(2(1 + \nu))$ ,  $G > 0$ , are defined in the classical way in terms of the Young's

modulus  $E$ ,  $E > 0$ , and Poisson ratio  $\nu$ ,  $\nu > 0$ . To complete the model, three additional materials constants,  $l_0 > 0$ ,  $l_1 > 0$ ,  $l_2 > 0$ , which account for scale effects are needed.

## 2.2. Modified strain gradient model for the axial vibrations of a uniform nanorod

Let us specialize the general modified strain gradient theory to the free longitudinal undamped vibrations of a slender straight uniform nanorod of length  $L$ , vibrating along its longitudinal axis  $x$ . Assuming the hypothesis of the simple theory of thin bars (i.e., rigid translation of the cross section along the  $x$  direction), the equation governing the axial displacement  $U(x, t)$  of the nanorod reads as, see [39] for details,

$$aU'''(x, t) - bU^{IV}(x, t) = \rho\ddot{U}(x, t), \quad (11)$$

where  $U'(x, t)$  and  $\dot{U}(x, t)$  indicate the first partial derivative of the function  $U$  with respect to  $x$  and  $t$ , respectively,  $x \in (0, L)$  and  $t > 0$ .

According to [39], the coefficient  $a$ ,  $a > 0$ , plays the role of the axial stiffness of the nanorod, and it can be conventionally expressed as  $a = EA$ . Here,  $A$  is a geometrical parameter, which, in analogy with classical large-scale rods, can be made coincident with the cross-sectional area of the nanorod. The coefficient  $\rho > 0$  is the constant mass per unit length. The coefficient  $b$  takes the expression

$$b = GA \left( 2l_0^2 + \frac{4}{5}l_1^2 \right). \quad (12)$$

Using the classical separation of variables method, the axial displacement  $U(x, t)$  can be expressed as

$$U(x, t) = u(x)e^{i\omega t}, \quad (13)$$

where  $u = u(x)$  is the amplitude of the normal mode (eigenfunction) associated to the natural (radian) frequency  $\omega$ . Substituting Eq.(13) into Eq.(11), the following ordinary differential equation is obtained

$$bu^{IV} - au'' = \lambda\rho u, \quad x \in (0, L), \quad (14)$$

$\lambda = \omega^2$  being the eigenvalue. We shall be concerned with the following sets of classical (left) and non-classical (right) boundary conditions.

#### **Clamped-Clamped (C-C)**

$$u(0) = 0, \quad u''(0) = 0, \quad (15)$$

$$u(L) = 0, \quad u''(L) = 0; \quad (16)$$

#### **Clamped-Free (C-F)**

$$u(0) = 0, \quad u''(0) = 0, \quad (17)$$

$$u'(L) = 0, \quad u'''(L) = 0; \quad (18)$$

#### **Free-Free (F-F)**

$$u'(0) = 0, \quad u'''(0) = 0, \quad (19)$$

$$u'(L) = 0, \quad u'''(L) = 0. \quad (20)$$

The non-classical end conditions selected above are only one of the possible sets of non-classical boundary conditions that may be assigned at the ends of a nanorod. Our choice is motivated by the fact that these boundary operators ensure the self-adjointness of the eigenvalue problem and, then, the reality of the eigenvalues. To show this, let  $\mathcal{D} = \left( b \frac{d^4}{dx^4} - a \frac{d^2}{dx^2} \right)$  be the nanorod operator in (14) and let us denote by  $\mathcal{B}$  a boundary operator either of the type  $(C - C)$ ,  $(C_F)$  or  $(F_F)$ , e.g., in case  $(C - C)$ ,  $\mathcal{B}u = 0$  means  $u(0) = u''(0) = 0 = u(L) = u''(L)$ . A direct calculation shows that  $\int_0^L (\mathcal{D}u)v = \int_0^L u(\mathcal{D}v)$  for every  $u, v \in C^4(0, L)$  for which  $\mathcal{B}u = \mathcal{B}v = 0$ , that is the pair  $\{\mathcal{D}, \mathcal{B}\}$  is self-adjoint.

The following properties of the eigenvalue problem (14), coupled with one of the boundary conditions (15)–(16), (17)–(18), (19)–(20) can be deduced from the general theory:

i) there exists an infinite sequence of real non-negative eigenvalues  $\{\lambda_n\}_{n=1}^{\infty}$ , with  $\lim_{n \rightarrow \infty} \lambda_n = \infty$ , all of which are simple.

ii) The family of the eigenfunctions  $\{u_n(x)\}_{n=1}^{\infty}$  is an orthogonal basis of the space of the admissible deformations of the nanorod.

iii) The  $n$ th eigenvalue of the nanorod differential equation (14), coupled with one set of boundary conditions of the type  $(C - C)$ ,  $(C - F)$  or  $(F - F)$ , is greater than the  $n$ th eigenvalue of the corresponding classical rod. The inequality is always strict, with the exception of the first (vanishing) eigenvalue of the case  $(F - F)$ . This property was already noticed in the literature (see, for example, Figure 5 and Figure 6 in [39]), and it is a consequence of the extremum properties of the eigenvalues [45]. The property follows by

noticing that an admissible deformation of the nanorod is also an admissible deformation of the classical rod, and that the strain energy density of the nanorod is bigger than the strain energy density of the classical rod, see the variational characterization of the eigenvalues given in (35)–(37) below.

Moreover, a direct inspection of the eigenvalue problem shows that if  $v$  is an eigenfunction of the classical rod (satisfying the differential equation (14) with  $b = 0$  and one set of classical boundary conditions of the type  $(C - C)$ ,  $(C - F)$  or  $(F - F)$ ), then  $v$  is also an eigenfunction of the nanorod under the same set of (classical and non-classical) end conditions; and vice versa.

The above general properties can be easily confirmed by the direct determination of the following closed form expressions of the eigenpairs of (14) coupled with one of the three boundary conditions  $(C - C)$ ,  $(C - F)$ ,  $(F - F)$ .

#### **Clamped-Clamped (C-C)**

$$u_n^{C-C}(x) = \sqrt{\frac{2}{\rho L}} \sin\left(\frac{n\pi x}{L}\right), \quad (21)$$

$$\lambda_n^{C-C} = \left(\frac{n\pi}{L}\right)^2 \left[ \frac{1}{\rho} \left( a + b \left(\frac{n\pi}{L}\right)^2 \right) \right], \quad n \geq 1; \quad (22)$$

#### **Clamped-Free (C-F)**

$$u_n^{C-F}(x) = \sqrt{\frac{2}{\rho L}} \sin\left(\frac{(2n-1)\pi x}{2L}\right), \quad (23)$$

$$\lambda_n^{C-F} = \left(\frac{(2n-1)\pi}{2L}\right)^2 \left[ \frac{1}{\rho} \left( a + b \left(\frac{(2n-1)\pi}{2L}\right)^2 \right) \right], \quad n \geq 1; \quad (24)$$

### Free-Free (F-F)

$$u_n^{F-F}(x) = \sqrt{\frac{2}{\rho L}} \cos\left(\frac{n\pi x}{L}\right), \quad (25)$$

$$\lambda_n^{F-F} = \left(\frac{n\pi}{L}\right)^2 \left[ \frac{1}{\rho} \left( a + b \left(\frac{n\pi}{L}\right)^2 \right) \right], \quad n \geq 0. \quad (26)$$

According to Eqs. (11) and (12),  $l_2$  does not play any role in the equation governing the axial displacement. Thus, the only material constants accounting for length scale effects are  $l_0$  and  $l_1$ , which are grouped in the parameter  $b$ . From the Eqs. (22), (24) and (26) it can be easily shown that increasing values of  $l_0$  or  $l_1$  leads to higher values of the natural frequencies.

### 2.3. Free axial vibrations of a uniform nanorod carrying a point mass

Basing on the conventional detection principle (see the Introduction), we assume that a point mass  $M$  is added at the cross-section of the nanorod of abscissa  $s$ ,  $s \in (0, L)$ , see Fig. 1. The differential operator governing the eigenvalue problem for the nanorod with a point mass is

$$b\tilde{u}^{IV} - a\tilde{u}'' = \tilde{\lambda}\rho\tilde{u}, \quad x \in (0, s) \cup (s, L), \quad (27)$$

where, in addition to one of the end conditions (15)–(16), (17)–(18), (19)–(20), we have also to consider the jump conditions at  $x = s$

$$\left\{ \begin{array}{l} [[\tilde{u}(s)]] = 0, \end{array} \right. \quad (28)$$

$$\left\{ \begin{array}{l} [[\tilde{u}'(s)]] = 0, \end{array} \right. \quad (29)$$

$$\left\{ \begin{array}{l} [[\tilde{u}''(s)]] = 0, \end{array} \right. \quad (30)$$

$$\left\{ \begin{array}{l} [[(a\tilde{u}' - b\tilde{u}''') (s)]] = -\tilde{\lambda}M\tilde{u}(s), \end{array} \right. \quad (31)$$

where  $[[\varphi(s)]] = (\varphi(s^+) - \varphi(s^-))$  denotes the jump of the function  $\varphi$  at  $x = s$ . The unperturbed nanorod clearly corresponds to  $M \rightarrow 0^+$ .

To solve the eigenvalue problem for the nanorod with a point mass we need to find a nontrivial  $\tilde{u} \in C^4((0, s) \cup (s, L)) \cap C^1((0, L))$  and  $\tilde{\lambda} \in \mathbb{R}^+$  such that (27)–(31) are satisfied, under a given set of end conditions.

In the sequel, we shall need the weak formulation of the eigenvalue problem. Let  $H^m(a, b)$ , with  $-\infty < a < b < +\infty$ , be the real-valued Hilbert space of the Lebesgue measurable functions  $f : (a, b) \rightarrow \mathbb{R}$  such that  $\int_a^b \left( f^2 + \sum_{i=1}^m \left( \frac{d^i f}{dx^i} \right)^2 \right) < +\infty$ , where  $\frac{d^i f}{dx^i}$  is the  $i$ th weak derivative of  $f$ . For the sake of simplicity, we shall consider the specific case of boundary conditions  $(C - C)$ . The other cases  $(C - F)$  and  $(F - F)$  can be managed similarly.

Let us multiply (27) by  $\varphi \in H^2((0, s) \cup (s, L))$  satisfying  $[[\varphi(s)]] = [[\varphi'(s)]] = 0$  and end conditions  $\varphi(0) = 0 = \varphi(L)$ . Integrating by parts twice, we have

$$\begin{aligned} b\tilde{u}''''\varphi \Big|_0^{s^-} + b\tilde{u}''''\varphi \Big|_{s^+}^L - b\tilde{u}'''\varphi' \Big|_0^{s^-} - b\tilde{u}'''\varphi' \Big|_{s^+}^L - a\tilde{u}''\varphi \Big|_0^{s^-} - a\tilde{u}''\varphi \Big|_{s^+}^L + \\ + \int_0^L (b\tilde{u}''\varphi'' + a\tilde{u}'\varphi') = \tilde{\lambda} \int_0^L \rho\tilde{u}\varphi \end{aligned} \quad (32)$$

Using the jump and end conditions on  $\tilde{u}$  at  $x = s$  and  $x = 0, L$ , respectively, and by the definition of  $\varphi$ , we get the weak formulation of (27)–(31) under  $(C - C)$  boundary conditions: to find  $\tilde{u} \in \mathcal{H} \setminus (0)$  and  $\tilde{\lambda} \in \mathbb{R}$  such that

$$\int_0^L (b\tilde{u}''\varphi'' + a\tilde{u}'\varphi') = \tilde{\lambda} \left( M\tilde{u}(s)\varphi(s) + \int_0^L \rho\tilde{u}\varphi \right), \quad \text{for every } \varphi \in \mathcal{H}, \quad (33)$$

where

$$\mathcal{H} = \{f : (0, L) \rightarrow \mathbb{R} \mid f \in H^2((0, s) \cup (s, L)), f(0) = 0 = f(L), [[f(s)]] = [[f'(s)]] = 0\}. \quad (34)$$

The Rayleigh's quotient  $R[\cdot]$  associated to the weak formulation (33)–(34) is

$$R : \mathcal{H} \setminus \{0\} \rightarrow \mathbb{R}^+, \quad R[\varphi] = \frac{\int_0^L b(\varphi'')^2 + a(\varphi')^2}{M\varphi^2(s) + \int_0^L \rho\varphi^2} \quad (35)$$

and the  $n$ th eigenpair  $(\tilde{\lambda}_n, \tilde{u}_n(x))$  is such that

$$\tilde{\lambda}_n = \min_{\varphi \in \mathcal{V}_n \setminus \{0\}} R[\varphi] = R[\tilde{u}_n], \quad n \geq 1, \quad (36)$$

where

$$\mathcal{V}_n = \left\{ f \in \mathcal{H} \mid Mf(s)\tilde{u}_i(s) + \int_0^L \rho f \tilde{u}_i dx = 0, \quad i = 1, \dots, n-1 \right\}. \quad (37)$$

It can be shown that properties i) and ii) mentioned above for the unperturbed nanorod apply also to the eigenvalue problem for the nanorod carrying a point mass. However, closed-form solutions for the eigenpairs are generally not available, even for the constant coefficient case.

### 3. Eigenvalue shifts induced by a small point mass: a perturbative approach

In this section we shall assume that the point mass  $M$  is small with respect to the total mass of the nanorod, i.e.,

$$M \ll \rho L. \quad (38)$$

Under this assumption, we shall investigate on the effects of the added mass on the eigenvalues of the nanorod. Again, to simplify the presentation, attention is focused on  $(C - C)$  end conditions. From the variational theory of eigenvalues recalled in (35)–(37), it easily follows that no natural frequency can be increased due to the addition of the point mass  $M$ , i.e.,

$$\tilde{\lambda}_n \leq \lambda_n, \quad \text{for every } n \geq 1. \quad (39)$$

However, in order to study the inverse problem of identifying the point mass by natural frequency data, we need quantitative information on the effects of the added mass. A first result is contained in the next statement.

**Proposition 3.1.** *Let  $(\tilde{\lambda}, \tilde{u})$  be an eigenpair of (33)–(34). Then, for a given position  $s \in (0, L)$  of the point mass,  $\tilde{\lambda} = \tilde{\lambda}(M)$  is a  $C^1$ -function in  $(0, \infty)$  and we have*

$$\frac{\partial \tilde{\lambda}}{\partial M} = -\tilde{\lambda} \frac{\tilde{u}^2(s)}{M\tilde{u}^2(s) + \int_0^L \rho \tilde{u}^2} \quad (40)$$

*Proof.* We apply to the weak formulation (33) the forward-difference operator

$$\delta_h f(x; M) = \frac{f(x; M+h) - f(x; M)}{h}, \quad h > 0, \quad M \in (0, \infty). \quad (41)$$

We have

$$\begin{aligned} \int_0^L (b(\delta_h \tilde{u}'') \varphi'' + a(\delta_h \tilde{u}') \varphi') &= \delta_h \tilde{\lambda} \left( M \tilde{u}(s) \varphi(s) + \int_0^L \rho \tilde{u} \varphi \right) + \\ &\tilde{\lambda} \left[ \tilde{u}(s) \varphi(s) + M (\delta_h \tilde{u}(s)) \varphi(s) + \int_0^L \rho (\delta_h \tilde{u}) \varphi \right], \end{aligned} \quad (42)$$

for every  $C^2$ -piecewise function  $\varphi$  in  $[0, L]$ , with  $\varphi(0) = 0 = \varphi(L)$ .

Let us take  $\varphi = \tilde{u}$  and let us note that  $\delta_h \tilde{u}$  is a suitable test function for the weak formulation of the problem. Then

$$\begin{aligned} \int_0^L (b(\delta_h \tilde{u}'') \tilde{u}'' + a(\delta_h \tilde{u}') \tilde{u}') &= \delta_h \tilde{\lambda} \left( M \tilde{u}^2(s) + \int_0^L \rho \tilde{u}^2 \right) + \\ &\tilde{\lambda} \tilde{u}^2(s) + \tilde{\lambda} \left[ M (\delta_h \tilde{u}(s)) \tilde{u}(s) + \int_0^L \rho (\delta_h \tilde{u}) \tilde{u} \right] \end{aligned} \quad (43)$$

The left hand side of (43) simplifies with the last square bracket on the right end side. Then, taking the limit as  $h \rightarrow 0^+$ , we obtain

$$\frac{\partial \tilde{\lambda}}{\partial M}(M^+) = -\tilde{\lambda} \frac{\tilde{u}^2(s)}{M \tilde{u}^2(s) + \int_0^L \rho \tilde{u}^2}. \quad (44)$$

By repeating the above analysis with the backward-difference operator  $\delta_{-h}(\cdot)$ , the left derivative of the eigenvalue  $\tilde{\lambda} = \tilde{\lambda}(M)$  turns out to be equal to the right derivative. Then, the function  $\tilde{\lambda} = \tilde{\lambda}(M)$  is continuously differentiable and (40) is proved.  $\square$

By adapting the arguments in [46], we can prove the following useful result.

**Theorem 3.2.** *There exists  $\widehat{M}, \widehat{M} > 0$ , such that the eigenvalues  $\tilde{\lambda}_n = \tilde{\lambda}_n(M)$  of (33)–(34) are holomorphic functions of  $M$ , for  $0 < M < \widehat{M}$ .*

By Proposition 3.1 and Theorem 3.2, and assuming the mass-normalization condition  $\int_0^L \rho u_n^2 = 1$ , the Taylor series expansion truncated to the first order term in the smallness parameter  $M$  for the  $n$ th eigenvalue is given by

$$\tilde{\lambda}_n(M) = \lambda_n - \lambda_n u_n^2(s) M. \quad (45)$$

Relation (45) shows that the change in an eigenvalue can be written as the product of the eigenvalue itself, the square of the corresponding (mass-normalized) eigenfunction of the unperturbed nanorod evaluated at the mass position, and the mass variation. Equation (45) plays an important role in our inverse problem, since it shows that the ratios of the relative changes in two different eigenvalues depend only on the location of the point mass, not on its magnitude, namely (if  $\delta\lambda_k < 0$ )

$$\frac{\frac{\delta\lambda_n}{\lambda_n}}{\frac{\delta\lambda_k}{\lambda_k}} = \frac{u_n^2(s)}{u_k^2(s)} \equiv f(s), \quad (46)$$

where  $\delta\lambda_n \equiv \tilde{\lambda}_n - \lambda_n$  and  $s \in (0, L)$ . Note that if  $\delta\lambda_k = 0$ , then the possible point mass location coincides with one of the node points of the  $k$ th vibrating mode  $u_k$  of the unperturbed nanorod. Therefore, the problem of localizing the point mass is reduced to the determination of the solutions of (46) for fixed/measured value of the ratio  $\frac{\delta\lambda_n}{\lambda_n} / \frac{\delta\lambda_k}{\lambda_k}$ . Let us observe that, once the unperturbed configuration is known, the function  $f = f(s)$  can be determined numerically or analytically. This idea was first explored in [47] for the identification of a point mass in a full-scale longitudinally vibrating rod under free-free end conditions, see also [48]. It should be noticed that the analysis developed in [47] and [48] deals with the identification of a point mass, described as a Dirac's delta, in a classical *second-order* Sturm-Liouville operator, whereas, as it was shown in Section 2, the longitudinal vibration of a nanorod involves a *fourth-order* differential operator.

In the next section we shall show that there are certain situations in which a suitable choice of the frequency input data allows obtaining closed

form solutions of the linearized inverse problem.

#### 4. Identification of a small point mass in uniform nanorods

We first consider the identification of the small point mass  $M$  in a nanorod under clamped-clamped end conditions ( $C - C$ ). Recalling the expressions of the eigenpairs (25)–(26), by (45) we have

$$C_n^{C-C} = M \sin^2 \left( \frac{n\pi s}{L} \right), \quad (47)$$

where

$$C_n^{C-C} = -\frac{\left( \tilde{\lambda}_n^{C-C} - \lambda_n^{C-C} \right) \rho L}{\lambda_n^{C-C}} \frac{1}{2}, \quad n \geq 1. \quad (48)$$

A direct calculation shows that

$$M \left( 4C_n^{C-C} - C_{2n}^{C-C} \right) = 4 \left( C_n^{C-C} \right)^2, \quad n \geq 1. \quad (49)$$

In order to identify the point mass, let us distinguish two cases.

*First case.* Let us assume  $C_n^{C-C} > 0$  (note that  $C_1^{C-C}$  is always strictly positive). By equation (49) we have

$$M = \frac{C_n^{C-C}}{1 - \frac{C_{2n}^{C-C}}{4C_n^{C-C}}}, \quad (50)$$

which gives a closed-form expression for the mass intensity  $M$  in terms of the ( $n$ th,  $2n$ th) eigenfrequency changes. It is worth noticing that, by (49),  $M$  in (50) takes positive values. The position of the point mass can be determined by inserting the expression (50) into (47), namely

$$S = \cos \left( \frac{2n\pi s}{L} \right) = \frac{C_{2n}^{C-C}}{2C_n^{C-C}} - 1, \quad (51)$$

where  $S \in [-1, 1]$ . By taking  $n = 1$  in (51), the ratio of the first frequency changes is sufficient for the localization of the point mass, up to a symmetrical position with respect to the mid-point of the nanorod.

*Second case.* If  $C_n^{C-C} = 0$  for certain  $n \geq 2$ , then from (47) we have  $S = 1$ , that is the point mass is located in one of the points of zero-sensitivity of the  $n$ th vibration mode.

The above analysis shows that the pair of natural frequencies  $n$ th and  $2n$ th plays a special role in the linearized inverse problem. In fact, if the  $n$ th frequency is sensitive to the point mass, that is  $C_n^{C-C} > 0$  or equivalently  $u_n^2(s) > 0$ , then the pair  $\{C_n^{C-C}, C_{2n}^{C-C}\}$  determines uniquely the mass intensity  $M$ . It is worth noticing that the expression for  $M$  is the same for all the pairs of values  $\{C_n^{C-C}, C_{2n}^{C-C}\}$ . Concerning the possible point mass locations, equation (51) shows that their number generally increases as the order  $n$  of the frequencies involved increases, which accounts for the recourse to "low" frequencies for solving the localization problem.

Summing up, we have shown that the measurement of the first two natural frequencies in a clamped-clamped nanorod allows for the unique identification of the point mass (except for symmetrical positions). This conclusion must be modified for nanorods under different boundary conditions. As an example, let us consider the identification of the point mass in a clamped free nanorod from the first and second eigenfrequency changes. By inserting the expressions (23)–(24) into (45) we have

$$C_1^{C-F} = M \sin^2\left(\frac{\pi s}{2L}\right), \quad C_2^{C-F} = M \sin^2\left(\frac{3\pi s}{2L}\right). \quad (52)$$

Let  $z = \cos\left(\frac{\pi s}{L}\right)$ , with  $z \in (-1, 1)$ . Then, recalling the identity  $\cos(3\alpha) = (4\cos^3\alpha - 3\cos\alpha)$ , we obtain the following non-linear system in terms of the two unknowns  $z$  and  $M$

$$\begin{cases} C_1^{C-F} = \frac{M}{2}(1 - z), & (53) \\ C_2^{C-F} = \frac{M}{2}(1 - 4z^3 + 3z). & (54) \end{cases}$$

A direct calculation shows that

$$(9C_1^{C-F} - C_2^{C-F}) = 2M(z - 1)^2(z + 2) > 0 \quad (55)$$

and the damage localization problem (46) for  $n = 2$  and  $k = 1$  is reduced to solving the polynomial equation

$$(1 + 2z)^2 = \chi, \quad z \in (-1, 1), \quad (56)$$

where, by (55),

$$\chi = \frac{C_2^{C-F}}{C_1^{C-F}} \in [0, 9]. \quad (57)$$

The existence and the number of solutions of (56) depend on the values of the parameter  $\chi$ . If  $\chi \in [1, 9)$ , then there exists a unique solution  $z_1 \in (0, 1)$ , which corresponds to  $s_1 \in (0, \frac{L}{2})$ . If  $\chi \in (0, 1)$ , then there are two distinct solutions of (56), say  $z_1 \in (-1, -\frac{1}{2})$  and  $z_2 \in (-\frac{1}{2}, 0)$ , which correspond to  $s_1 \in (\frac{2L}{3}, L)$  and  $s_2 \in (\frac{L}{2}, \frac{2L}{3})$ , respectively. Finally, for  $\chi = 0$  equation (56) has a double zero at  $z = -\frac{1}{2}$ , corresponding to  $s = \frac{2L}{3}$ . In conclusion, should the point mass be located within the left half of the rod adjacent to the clamped end, the measurement of the first and second natural frequencies determines uniquely the location of the point mass. Conversely, should the

mass be located in the right half of the rod, there are two different locations corresponding to the same value  $\chi$ , apart when  $\chi = 0$ , which corresponds to the mass position at  $s = \frac{2}{3}L$ .

We conclude this section with the analysis of natural frequency data coming from two sets of different end conditions. It turns out that the measurement of the  $n$ th resonant frequency under boundary conditions  $(C - C)$  and the  $n$ th natural frequency under boundary conditions  $(F - F)$ ,  $n \geq 1$ , determines uniquely the point mass and the location variable  $S = \cos\left(\frac{2m\pi s}{L}\right)$ . In particular, by adopting the above procedure, we have

$$M = C_n^{F-F} + C_n^{C-C} \quad (58)$$

and

$$\text{if } C_n^{F-F} > 0, \quad \text{then } S = -1 + \frac{2}{1 + \frac{C_n^{C-C}}{C_n^{F-F}}}; \quad (59)$$

$$\text{if } C_n^{F-F} = 0, \quad \text{then } S = -1. \quad (60)$$

Here,  $C_n^{F-F} = -\frac{(\tilde{\lambda}_n^{F-F} - \lambda_n^{F-F})}{\lambda_n^{F-F} \frac{2}{\rho L}}$ ,  $n \geq 1$ . It follows that the point mass is uniquely determined (except for symmetrical positions) by  $\{C_1^{C-C}, C_1^{F-F}\}$ .

## 5. Applications

### 5.1. Exact versus perturbative solution

This section is devoted to the evaluation of the accuracy of the perturbation approach outlined in Section 3 in estimating the eigenvalues of the problem (27)–(31) with boundary conditions given either by (15)–(16)  $(C - C)$  or by (17)–(18)  $(C - F)$ . From the practical point of view, the free-free case

$(F - F)$  does not seem to be very suitable for nanosensors applications, and will not be considered in the sequel.

Following [39], we considered a nanorod with circular cross-section with diameter  $D$  and length  $L = 20D$ . Moreover, the two scale parameters  $l_0$  and  $l_1$  have been assumed to be equal, e.g.,  $l_0 = l_1 = l$ , and the selected Poisson's ratio was  $\nu = 0.38$ . The variation of the first three eigenvalues,  $\tilde{\lambda}_1, \tilde{\lambda}_2, \tilde{\lambda}_3$  (normalized to the corresponding eigenvalues  $\lambda_{0n}$  of the "classical" local rod, that is the rod with  $b = 0$ , without any attached mass) with respect to the intensity  $M$  of the point mass (normalized to the total mass of the nanorod  $\rho L$ ) has been calculated for various positions  $s$  and for  $D/l = \{2.0, 1.0, 0.5, 0.4\}$ .

Eigenfrequency changes have been obtained using both exact and perturbative solutions. The exact solution is calculated from the corresponding frequency equation in terms of nondimensional eigenvalue  $\Lambda = \frac{\rho L^2}{EA} \tilde{\lambda}$ , and nondimensional attached mass  $\bar{M} = \frac{M}{\rho L}$ .

For the case of a clamped-clamped nanorod the frequency equation reads as

$$f^{C-C}(\Lambda) = -\beta \sinh(\beta) (\alpha h^2 (\alpha^2 + \beta^2) \sin(\alpha) - \Lambda \bar{M} \sin(\alpha s) \sin(\alpha(1-s))) - \alpha \Lambda \bar{M} \sin(\alpha) \sinh(s\beta) \sinh(\beta(1-s)) = 0, \quad (61)$$

where the parameters  $\alpha$  and  $\beta$  are given by

$$\alpha = \sqrt{\frac{\sqrt{4h^2\Lambda + 1} - 1}{2h^2}}, \quad (62)$$

$$\beta = \sqrt{\frac{\sqrt{4h^2\Lambda + 1} + 1}{2h^2}}, \quad (63)$$

and  $h$  is the dimensionless parameter related to the length scale  $l$  by the following expression:

$$h = \sqrt{\frac{7}{5(1+\nu)} \frac{l}{20D}}. \quad (64)$$

The frequency equation for the clamped-free nanorod is

$$\begin{aligned} f^{C-F}(\Lambda) = \beta \cosh(\beta) (\alpha h^2 (\alpha^2 + \beta^2) \cos(\alpha) - \Lambda \bar{M} \sin(\alpha s) \cos(\alpha(1-s)) + \\ + \alpha \Lambda \bar{M} \cos(\alpha) \sinh(s\beta) \cosh(\beta(1-s\beta))) = 0. \end{aligned} \quad (65)$$

The first order change in eigenvalues is determined from (45), where  $u_n$  and  $\lambda_n$  are given by (21)–(22) and (23)–(24) for  $(C-C)$  and  $(C-F)$  end conditions, respectively.

Figs. 2 to 4 show, for the  $(C-C)$  boundary conditions, the variation of the first three eigenvalues with the attached mass located at different positions and for the selected values of  $D/l$ . For moderate values of the attached mass, i.e.  $M/\rho L \in [0, 0.2]$ , there is a good agreement between exact and first-order solution. For the fundamental mode, for example, the accuracy generally decreases as the mass location moves toward the mid-point of the nanorod. In fact, the maximum difference is encountered at  $s = \frac{l}{2}$ , and it

oscillates between 15 and 22 percent. As it was observed above, in absence of the attached mass, eigenfrequency values of the strain gradient nanorod are higher than those of the classical rod model, and they increase when the scale parameter  $l$  increases ( $D/l$  decreases), meaning that the generalized constitutive model used leads to a stiffening of the structure.

The results corresponding to clamped-free boundary conditions are shown in Figs. 5 to 7, and considerations analogous to the clamped-clamped case can be made. In the case of the fundamental mode, the maximum difference between exact and perturbative results occurs for mass location  $s = 0.9$ , and its value is about 16 percent.

### *5.2. Solution of the inverse problem*

In this section some results on the capability of the method proposed in Section 4 to identify the value of the attached mass and its position are presented. For the clamped-clamped nanorod, among several simulations, the cases with mass intensity  $M/(\rho L) \in \{0.001, 0.025, 0.050, 0.100, 0.200\}$  and position  $s/L \in \{0.1, 0.25, 0.40, 0.50\}$  shall be considered in detail. It should be noticed that positions  $s/L > 1/2$  are not considered given the symmetry of the problem. The attached mass is identified using equations (48) and (50), while the position is obtained from equation (51). Table 1 collects the results when the first two natural frequencies are used in the identification process, i.e., for  $n = 1$ . It can be seen that, for small masses, the error in the identification of position and mass intensity remains at relatively small values. The case  $s/L = 0.50$  deserves special attention, since the position

is exactly identified. Larger errors are observed when the mass intensity increases.

Similar information is given in Table 2, in which the second and fourth frequencies are used (i.e.,  $n = 2$ ). Besides the fact that two possible solutions for the mass position can exist, the comparison of the values with those given in Table 1 shows that the precision in the identification of position and mass decreases, even for the identified location closest to the right one (except when  $s = 0.25$ , for which the method gives the exact solution). Specifically, for  $s = 0.5$  the identification method leads to imaginary values since this position coincides with a node of both the second and fourth shape modes, thus both the second and the fourth frequencies are insensitive to the presence of the point mass.

In the case of the clamped-free rod, as explained in the second part of Section 4, a different scenario is found. The method was tested for the same point mass intensities considered in the previous case, and the positions investigated covered the whole span of the rod, namely  $s = \{0.10, 0.35, 0.50, 0.65, 0.90\}$ , since the symmetry conditions do not hold for the clamped-free case. The mass location has been determined by solving (56). In agreement with the theory (e.g., case in which  $s \in (0, \frac{L}{2})$ ), for  $s = 0.10$  and  $s = 0.35$  only one solution is encountered in the identification process (see Table 3). The errors are moderate and increase with the attached mass intensity. For the other positions considered in simulations, two possible solutions are obtained,  $Sln.1$  and  $Sln.2$  (see Table 4), which correspond to  $s_1 \in (\frac{2L}{3}, L)$ , and  $s_2 \in (\frac{L}{2}, \frac{2L}{3})$ , respectively. In every case, as expected from the theory developed in the sec-

ond part of Section 4, one of these two solutions is close to the true solution, the other is spurious and follows from the non-uniqueness of the mathematical inverse problem. In all the cases, the mass intensity  $M$  was estimated by solving (55). It should be noticed that, for the sake of brevity, all the results quoted correspond to  $D/l = 0.4$ , the higher value of the scale parameter  $l$  considered in this study.

In order to evaluate the effect of errors on the data measurements, the 1st and 2nd eigenfrequencies were perturbed for a clamped-clamped nanorod ( $C-C$ ) with point mass intensity  $M/\rho L = 0.025$  at  $s = 0.4L$ , according to the expressions

$$\sqrt{\tilde{\lambda}_1^{pert}} = \sqrt{\tilde{\lambda}_1(1 + \tau_1)}; \quad \sqrt{\tilde{\lambda}_2^{pert}} = \sqrt{\tilde{\lambda}_2(1 + \tau_2)}, \quad (66)$$

where  $\tau_1$  and  $\tau_2$  are real random Gaussian variables with zero mean and standard deviations  $\sigma_1$  and  $\sigma_2$ , respectively. The maximum measurement error has been taken to be approximately equal to a given percentage  $II$ ,  $II = 5, 10, 15, 20\%$  of the frequency shift  $\delta\lambda_n$ , for  $n = 1, 2$ . Then, the standard deviations are defined as  $3\sigma_n = \delta\lambda_n II/100$ , for  $n = 1, 2$ . A MonteCarlo simulation on a population of 10000 samples was performed, leading to the results presented in Table 5, where the mean and standard deviations for the identification errors corresponding to mass intensity and position are shown for different values of the measurement error  $II$ . As it can be seen, the mean errors keep (approximately) constant with  $II$ , and equal to the corresponding identification errors shown in Table 1. Regarding the standard deviation, it increases with the measurement error, but keeps at a rather low value up to

$H = 0.20$ . All this confirms the robustness of the proposed method.

## 6. Concluding remarks

In this paper we obtained the natural frequencies of the axial vibrations of a nanorod carrying a concentrated mass through its span for both clamped-clamped and clamped-free end conditions. The modified strain gradient theory proposed in [31] has been used to take into account the size effects present in this kind of structures. The influence of the mass intensity, mass location, as well as the value of scale parameter have been analysed. For the case of small intensity of the concentrated mass, a first order perturbative technique is used to compute the natural frequencies of the nanorod. To our knowledge, this problem, which is relevant regarding application of nanostructures as sensors, is addressed for the first time. In fact, from the properties of the eigenvalue perturbative theory, the identification of a single point mass in a uniform nanorod (mass intensity and position) by minimal frequency data has been considered. We have shown that the point mass can be uniquely identified (up to a symmetrical position) by the knowledge of the first two natural frequencies of the nanorod under clamped-clamped end conditions.

Moreover, the effect of the frequency measurement errors on the estimated variables (mass intensity and location) has been illustrated with a statistical analysis, showing the robustness of the identification method. The results obtained herein encourage the use of axial vibrations of nanorods as a very precise sensing technique.

As a final remark, we point out that a problem worth of investigation that

emerges from the present analysis stands on the possibility of identifying a point mass of finite - not necessarily small - magnitude. It is likely that the results and methods presented in [49, 50] may be useful for this purpose.

### **Acknowledgement**

The authors wish to acknowledge *Ministerio de Economía y Competitividad de España* for the financial support, under grant number DPI2014-57989-P. The first author also gratefully acknowledges the financial support of the National Research Project PRIN2015 'Identificazione e diagnostica di sistemi strutturali complessi'.

## References

- [1] K. Eom, H. S. Park, D. S. Yoon, T. Kwon, Nanomechanical resonators and their applications in biological/chemical detection: Nanomechanics principles, *Physics Reports* 503 (2011) 115–163.
- [2] Q. Wang, B. Arash, A review on applications of carbon nanotubes and graphenes as nano-resonator sensors, *Computational Materials Science* 82 (2014) 350–360.
- [3] B. Arash, J. W. Jiang, T. Rabczuk, A review on nanomechanical resonators and their applications in sensors and molecular transportation, *Applied Physics Reviews* 2 (2015) 021301.
- [4] V. K. Khanna, *Nanosensors: Physical, Chemical, and Biological*, CRC Press, Boca raton, FL, 2012.
- [5] J. Tamayo, D. Ramos, J. Mertens, M. Calleja, Effect of the adsorbate stiffness on the resonance response of microcantilever sensors, *Applied Physics Letters* 89 (2006) 224104.
- [6] C. Wei, D. Srivastava, Nanomechanics of carbon nanofibers: Structural and elastic properties, *Applied Physics Letters* 85 (2004) 2208—2210.
- [7] X. Q. He, K. M. Liew, C. Wei, Mechanical properties of carbon nanocones, *Applied Physics Letters* 91 (2007) 261906–261906–3.
- [8] K. M. Liew, J. X. Wei, X. Q. He, Carbon nanocones under compression:

Buckling and post-buckling behaviors, *Physical Review B- Condensed Matter and Materials Physics* 75 (2007) 195435.

- [9] P. Tsai, T. Fang, A molecular dynamics study of the nucleation, thermal stability and nanomechanics of carbon nanocones, *Nanotechnology* 18 (2007) 105702.
- [10] E. Cosserat, F. Cosserat, *Theory of Deformable Bodies*, (Translated by D.H. Delphenich), Scientific Library, A. Hermann and Sons, Paris, 1909.
- [11] R. D. Mindlin, Micro-structure in linear elasticity, *Archive for Rational Mechanics and Analysis* 16 (1964) 51–78.
- [12] R. D. Mindlin, Second gradient of strain and surface-tension in linear elasticity, *International Journal of Solids and Structures* 1 (1965) 417–438.
- [13] A. C. Eringen, Linear theory of nonlocal elasticity and dispersion of plane-waves, *International Journal of Engineering Science* 10 (5) (1972) 233–248.
- [14] A. C. Eringen, D. G. B. Edelen, Nonlocal elasticity, *International Journal of Engineering Science* 10 (3) (1972) 233–248.
- [15] A. C. Eringen, On differential-equations of nonlocal elasticity and solutions of screw dislocation and surface-waves, *Journal of Applied Physics* 54 (9) (1983) 4703–4710.

- [16] J. Peddieson, G. R. Buchanan, R. P. McNitt, Application of nonlocal continuum models to nanotechnology, *International Journal of Engineering Science* 41 (3-5) (2003) 305–312.
- [17] H. Rafii-Tabar, E. Ghavanloo, S. A. Fazelzadeh, Nonlocal continuum-based modeling of mechanical characteristics of nanoscopic structures, *Physics Reports* 638 (2016) 1–97.
- [18] M. A. Eltaher, M. A. Agwa, F. F. Mahmoud, Nanobeam sensor for measuring a zeptogram mass, *International Journal of Mechanics and Materials in Design* 12 (2016) 211–221.
- [19] T. Murmu, S. Adhikari, Nonlocal frequency analysis of nanoscale biosensors, *Sensors and Actuators A: Physical* 173 (2012) 41–48.
- [20] X. F. Li, G. J. Tang, Z. B. Shen, K. Lee, Resonance frequency and mass identification of zeptogram-scale nanosensor based on the nonlocal beam theory, *Ultrasonics* 55 (2015) 75–84.
- [21] M. Aydogdu, S. Filiz, Modeling carbon nanotube-based mass sensors using axial vibration and nonlocal elasticity, *Physica E: Low-dimensional Systems and Nanostructures* 43 (2011) 1229–1234.
- [22] X. F. Li, G. J. Tang, Z. B. Shen, K. Y. Lee, Size-dependent resonance frequencies of longitudinal vibration of a nonlocal Love nanobar with a tip nanoparticle, *Mathematics and Mechanics of Solids* (2016) doi: 10.1177/1081286516640597.

- [23] E. Benvenuti, A. Simone, One-dimensional nonlocal and gradient elasticity: Closed-form solution and size effect, *Mechanics Research Communications* 48 (2013) 46–51.
- [24] Q. Wang, K. M. Liew, Application of nonlocal continuum mechanics to static analysis of micro- and nano-structures, *Physics Letters A* 363 (3) (2007) 236–242, wang, Q. Liew, K.M.
- [25] N. Challamel, C. M. Wang, The small length scale effect for a non-local cantilever beam: a paradox solved, *Nanotechnology* 19 (2008) 345703(7).
- [26] C. Wang, S. Kitipornchai, C. Lim, M. Eisenberger, Beam bending solutions based on nonlocal Timoshenko beam theory, *Journal of Engineering Mechanics* 134 (6) (2008) 475–481.
- [27] N. Challamel, Z. Zhang, C. M. Wang, J. N. Reddy, Q. Wang, T. Micheli, B. Collet, On nonconservativeness of Eringen’s nonlocal elasticity in beam mechanics: correction from a discrete-based approach, *Archive of Applied Mechanics* 84 (2014) 1275 – 1292.
- [28] P. Lu, H. P. Lee, C. Lu, P. Q. Zhang, Dynamic properties of flexural beams using a nonlocal elasticity model, *Journal of Applied Physics* 99 (2006) 1 – 9.
- [29] J. Fernández-Sáez, R. Zaera, J. A. Loya, J. N. Reddy, Bending of Euler-Bernoulli beams using Eringen’s integral formulation: A paradox resolved, *International Journal of Engineering Science* 99 (2016) 107–116.

- [30] G. Romano, R. Barretta, M. Diaco, F. Marotti de Sciarra, Constitutive boundary conditions and paradoxes in nonlocal elastic nanobeams, *International Journal of Mechanical Sciences* 121 (2017) 151–156.
- [31] D. C. C. Lam, F. Yang, A. C. M. Chong, J. Wang, P. Tong, Experiments and theory in strain gradient elasticity, *Journal of the Mechanics and Physics of Solids* 51 (2003) 1477–1508.
- [32] N. A. Fleck, J. W. Hutchinson, Strain gradient plasticity, *Advances in Applied Mechanics* 33 (1997) 295–361.
- [33] S. Kong, S. Zhou, Z. Nie, K. Wang, Static and dynamic analysis of micro-beams based on strain gradient elasticity theory, *International Journal of Engineering Science* 47 (2009) 487–498.
- [34] B. Wang, J. Zhao, S. Zhou, A microscale Timoshenko beam model based on strain gradient elasticity theory, *European Journal of Mechanics A-Solids* 29 (2010) 837–843.
- [35] B. Akgoz, O. Civalek, Strain gradient elasticity and modified couple stress models for buckling analysis of axially loaded micro-scaled beams, *International Journal of Engineering Science* 49 (2011) 1268–1280.
- [36] B. Akgoz, O. Civalek, A new trigonometric beam model for buckling of strain gradient microbeams, *International Journal of Mechanical Sciences* 81 (2014) 88–94.

- [37] M. Kahrobaian, S. Tajalli, M. Movahhedy, J. Akbari, M. Ahmadian, Torsion of strain gradient bars, *International Journal of Engineering Science* 49 (2011) 856–866.
- [38] S. Narendar, S. Gopalakrishnan, Strain gradient torsional vibration analysis of micro/nano rods, *International Journal of Nano Dimension* 3 (2012) 1–17.
- [39] B. Akgoz, O. Civalek, Longitudinal vibration analysis for microbars based on strain gradient elasticity theory, *Journal of Vibration and Control* 20 (2014) 606–616.
- [40] B. Akgoz, O. Civalek, Longitudinal vibration analysis of strain gradient bars made of functionally graded materials(FGM), *Composites: Part B* 55 (2013) 263–268.
- [41] U. Guven, Love-Bishop rod solution based on strain gradient elasticity theory, *Comptes Rendus Mecanique* 342 (2014) 8–16.
- [42] K. Yu, P. Zijlstra, J. E. Sader, Q.-H. Xu, M. Orrit, Damping of Acoustic Vibrations of Immobilized Single Gold Nanorods in Different Environments, *Nano Letters* 13 (6) (2013) 2710–2716.
- [43] M. A. Mahmoud, D. O’Neil, M. A. El-Sayed, Shape- and Symmetry-Dependent Mechanical Properties of Metallic Gold and Silver on the Nanoscale, *Nano Letters* 14 (2) (2014) 743–748.

- [44] P. Guo, R. D. Schaller, L. E. Ocola, J. B. Ketterson, R. P. H. Chang, Gigahertz Acoustic Vibrations of Elastically Anisotropic Indium-Tin-Oxide Nanorod Arrays, *Nano Letters* 16 (9) (2016) 5639–5646.
- [45] R. Courant, D. Hilbert, *Methods of Mathematical Physics*, (first English edition) ed., Interscience Publishers Inc., New York, 1966.
- [46] T. Kato, *Perturbation Theory for Linear Operators*, Springer, Berlin, Germany, 1995.
- [47] A. Morassi, M. Dilella, On point mass identification in rods and beams from minimal frequency measurements, *Inverse Problems in Engineering* 10 (2002) 183–201.
- [48] A. Akhlyamov, A. Ayupova, Point mass identification in rods, *Russian Journal of Nondestructive Testing* 49 (2013) 572–578.
- [49] L. Rubio, J. Fernandez-Saez, A. Morassi, Crack identification in non-uniform rods by two frequency data, *International Journal of Solids and Structures* 75-76 (2015) 61–80.
- [50] J. Fernandez-Saez, A. Morassi, M. Pressacco, L. Rubio, Unique determination of a single crack in a uniform simply supported beam in bending vibration, *Journal of Sound and Vibration* 371 (2016) 94–109.

## Table Captions

Table 1. Identification of the mass intensity  $M$  and position  $s$  in a clamped-clamped nanorod ( $C - C$ ) from the first and second natural frequencies.  $D/l = 0.4$ . Percentage errors:  $e_s = 100 \times (s_{est} - s)/s$ ,  $e_M = 100 \times (M_{est} - M)/M$ .

Table 2. Identification of the mass intensity  $M$  and position  $s$  in a clamped-clamped nanorod ( $C - C$ ) from the second and fourth natural frequencies.  $D/l = 0.4$ . Existence of two solutions for the mass position ( $e_{s1}$  and  $e_{s2}$ ). Percentage errors:  $e_s = 100 \times (s_{est} - s)/s$ ,  $e_M = 100 \times (M_{est} - M)/M$ . \*: no results.

Table 3. Identification of the mass intensity  $M$  and position  $s$  in a clamped-free nanorod ( $C - C$ ) from the first and second natural frequencies.  $D/l = 0.4$ .  $s \in (0, \frac{L}{2})$ : existence of unique solution. Percentage errors:  $e_s = 100 \times (s_{est} - s)/s$ ,  $e_M = 100 \times (M_{est} - M)/M$ .

Table 4. Identification of the mass intensity  $M$  and position  $s$  in a clamped-free nanorod ( $C - F$ ) from the first and second natural frequencies.  $D/l = 0.4$ .  $s \in [\frac{L}{2}, L]$ : existence of two solutions (*Sln.1* and *Sln.2*). Percentage errors:  $e_s = 100 \times (s_{est} - s)/s$ ,  $e_M = 100 \times (M_{est} - M)/M$ .

Table 5. Mean and standard deviation for the errors corresponding to the identification of mass intensity and position from the first and second natural frequencies, as a function of the frequency measurement error. Clamped-clamped nanorod ( $C - C$ ) with  $M/\rho L = 0.025$  and  $s = 0.4L$ .

## Figure Captions

Figure 1. Nanorod with a point mass  $M$  located at abscissa  $s$  under different boundary conditions. (a) Clamped-clamped; (b) clamped-free.

Figure 2. Clamped-clamped nanorod. Normalized first eigenvalue versus dimensionless point-mass, for different mass positions, and different values of the length scale parameter.

Figure 3. Clamped-clamped nanorod. Normalized second eigenvalue versus dimensionless point-mass, for different mass positions, and different values of the length scale parameter.

Figure 4. Clamped-clamped nanorod. Normalized third eigenvalue versus dimensionless point-mass, for different mass positions, and different values of the length scale parameter.

Figure 5. Clamped-free nanorod. Normalized first eigenvalue versus dimensionless point-mass, for different mass positions, and different values of the length scale parameter.

Figure 6. Clamped-free nanorod. Normalized second eigenvalue dimensionless point-mass, for different mass positions, and different values of the length scale parameter.

Figure 7. Clamped-free nanorod. Normalized third eigenvalue dimensionless point-mass, for different mass positions, and different values of the length scale parameter.

Table 1: Identification of the mass intensity  $M$  and position  $s$  in a clamped-clamped nanorod ( $C - C$ ) from the first and second natural frequencies.  $D/l = 0.4$ . Percentage errors:  $e_s = 100 \times (s_{est} - s)/s$ ,  $e_M = 100 \times (M_{est} - M)/M$ .

$\frac{M}{\rho L}$	$s = 0.10L$		$s = 0.25L$		$s = 0.40L$		$s = 0.50L$	
	$e_s$	$e_M$	$e_s$	$e_M$	$e_s$	$e_M$	$e_s$	$e_M$
0.010	0.18	-0.24	1.34	-2.54	0.09	-1.62	0	-1.83
0.025	0.61	-0.91	3.26	-6.04	0.22	-3.97	0	-4.46
0.050	1.72	-2.76	6.21	-11.16	0.42	-7.68	0	-8.56
0.100	5.37	-8.70	11.29	-19.37	0.77	-14.39	0	-15.85
0.200	17.06	-24.74	18.95	-30.85	1.34	-25.49	0	-27.54

Table 2: Identification of the mass intensity  $M$  and position  $s$  in a clamped-clamped nanorod ( $C - C$ ) from the second and fourth natural frequencies.  $D/l = 0.4$ . Existence of two solutions for the mass position ( $e_{s1}$  and  $e_{s2}$ ). Percentage errors:  $e_s = 100 \times (s_{est} - s)/s$ ,  $e_M = 100 \times (M_{est} - M)/M$ . \*: no results.

$\frac{M}{\rho L}$	$s = 0.10L$			$s = 0.25L$			$s = 0.40L$			$s = 0.50L$		
	$e_{s1}$	$e_{s2}$	$e_M$	$e_{s1}$	$e_{s2}$	$e_M$	$e_{s1}$	$e_{s2}$	$e_M$	$e_{s1}, e_{s2}$	$e_M$	
0.010	2.65	297.35	-4.34	0	0	-2.59	-74.38	-0.62	-6.28	*	*	
0.025	6.65	293.35	-10.31	0	0	-6.29	-73.53	-1.47	-14.23	*	*	
0.050	13.19	286.81	-18.78	0	0	-12.00	-72.31	-72.31	-24.62	*	*	
0.100	25.02	274.98	-31.01	0	0	-21.88	-70.43	-70.43	-38.84	*	*	
0.200	42.72	257.28	-44.49	0	0	-36.80	-68.0	-68.01	-54.90	*	*	

Table 3: Identification of the mass intensity  $M$  and position  $s$  in a clamped-free nanorod ( $C - F$ ) from the first and second natural frequencies.  $D/l = 0.4$ .  $s \in (0, \frac{L}{2})$ : existence of unique solution. Percentage errors:  $e_s = 100 \times (s_{est} - s)/s$ ,  $e_M = 100 \times (M_{est} - M)/M$ .

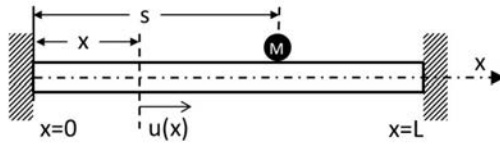
$\frac{M}{\rho L}$	$s = 0.10L$		$s = 0.35L$	
	$e_s$	$e_M$	$e_s$	$e_M$
0.010	-0.68	1.42	0.94	-2.00
0.025	-1.88	3.94	2.29	-4.79
0.050	-3.59	7.72	4.40	-8.97
0.100	-6.18	13.87	8.12	-15.91
0.200	-7.83	18.34	14.05	-26.05

Table 4: Identification of the mass intensity  $M$  and position  $s$  in a clamped-free nanorod ( $C - F$ ) from the first and second natural frequencies.  $D/l = 0.4$ .  $s \in [\frac{L}{2}, L]$ : existence of two solutions ( $Sln.1$  and  $Sln.2$ ). Percentage errors:  $e_s = 100 \times (s_{est} - s)/s$ ,  $e_M = 100 \times (M_{est} - M)/M$ .

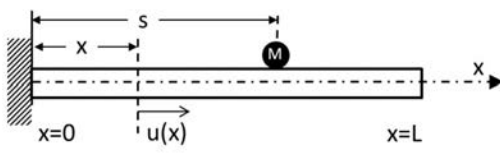
$\frac{M}{\rho L}$	$s = 0.50L$						$s = 0.65L$						$s = 0.90L$					
	$Sln.1$		$Sln.2$		$Sln.1$		$Sln.2$		$Sln.1$		$Sln.2$		$Sln.1$		$Sln.2$			
	$e_s$	$e_M$	$e_s$	$e_M$	$e_s$	$e_M$	$e_s$	$e_M$	$e_s$	$e_M$	$e_s$	$e_M$	$e_s$	$e_M$	$e_s$	$e_M$		
0.010	96.19	-50.39	0.11	-1.04	5.22	-7.26	-0.01	-1.38	-0.38	-1.58	-42.59	82.16						
0.025	94.00	-50.96	0.28	-2.57	5.23	-9.16	-0.02	-3.37	-0.91	-3.87	-42.42	76.67						
0.050	91.59	-51.89	0.55	-5.03	5.24	-12.16	-0.03	-6.53	-1.66	-7.49	-42.16	68.21						
0.100	88.32	-53.67	1.07	-9.64	5.27	-17.63	-0.06	-12.28	-2.84	-14.08	-41.73	53.47						
0.200	84.11	-56.92	1.97	-17.72	5.33	-26.79	-0.11	-21.94	-4.42	-25.02	-41.09	30.48						

Table 5: Mean and standard deviation for the errors corresponding to the identification of mass intensity and position from the first and second natural frequencies, as a function of the frequency measurement error. Clamped-clamped nanorod ( $C-C$ ) with  $M/\rho L = 0.025$  and  $s = 0.4L$ .

Measurement Error, $H$ (%)	Mass mean error (%)	Mass standard dev.	Position mean error (%)	Position standard dev.
5	-3.970	$1.05 \cdot 10^{-4}$	0.217	$2.71 \cdot 10^{-4}$
10	-3.962	$2.09 \cdot 10^{-4}$	0.217	$5.39 \cdot 10^{-4}$
15	-3.957	$3.11 \cdot 10^{-4}$	0.217	$8.10 \cdot 10^{-4}$
20	-3.983	$4.20 \cdot 10^{-4}$	0.211	$10.84 \cdot 10^{-4}$



(a)



(b)

Figure 1: Nanorod with a point mass  $M$  located at abscissa  $s$  under different boundary conditions. (a) Clamped-clamped; (b) clamped-free.

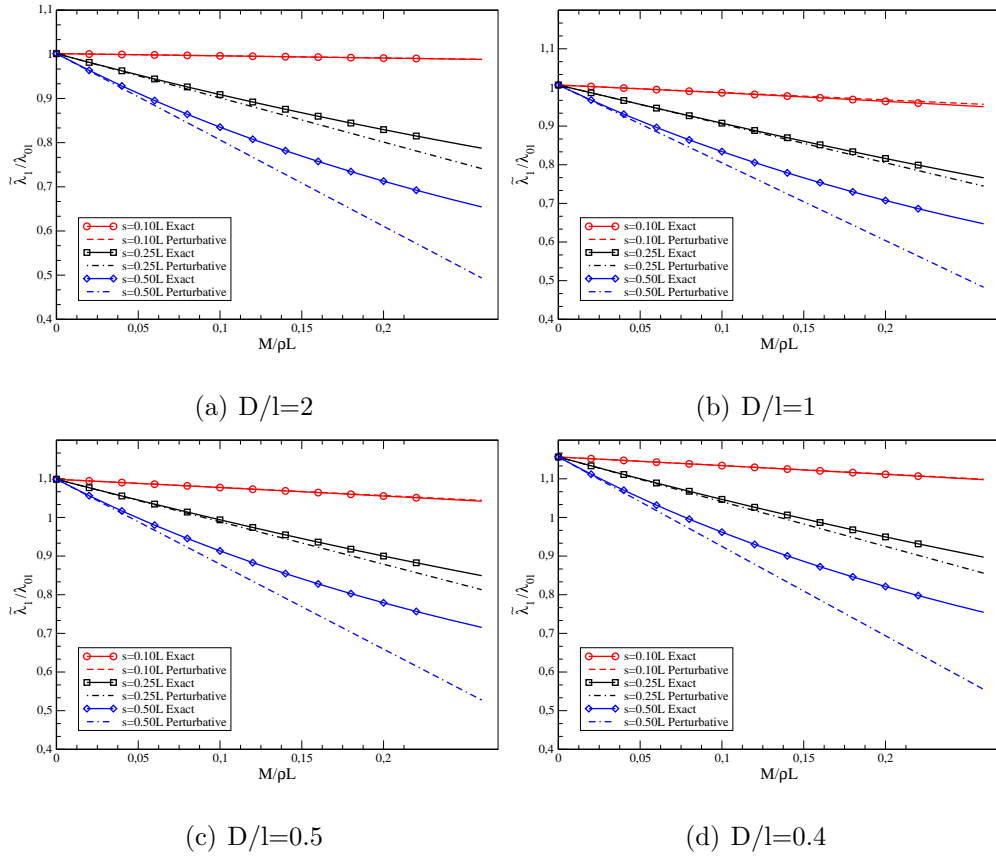


Figure 2: Clamped-clamped nanorod. Normalized first eigenvalue versus dimensionless point-mass, for different mass positions, and different values of the length scale parameter.

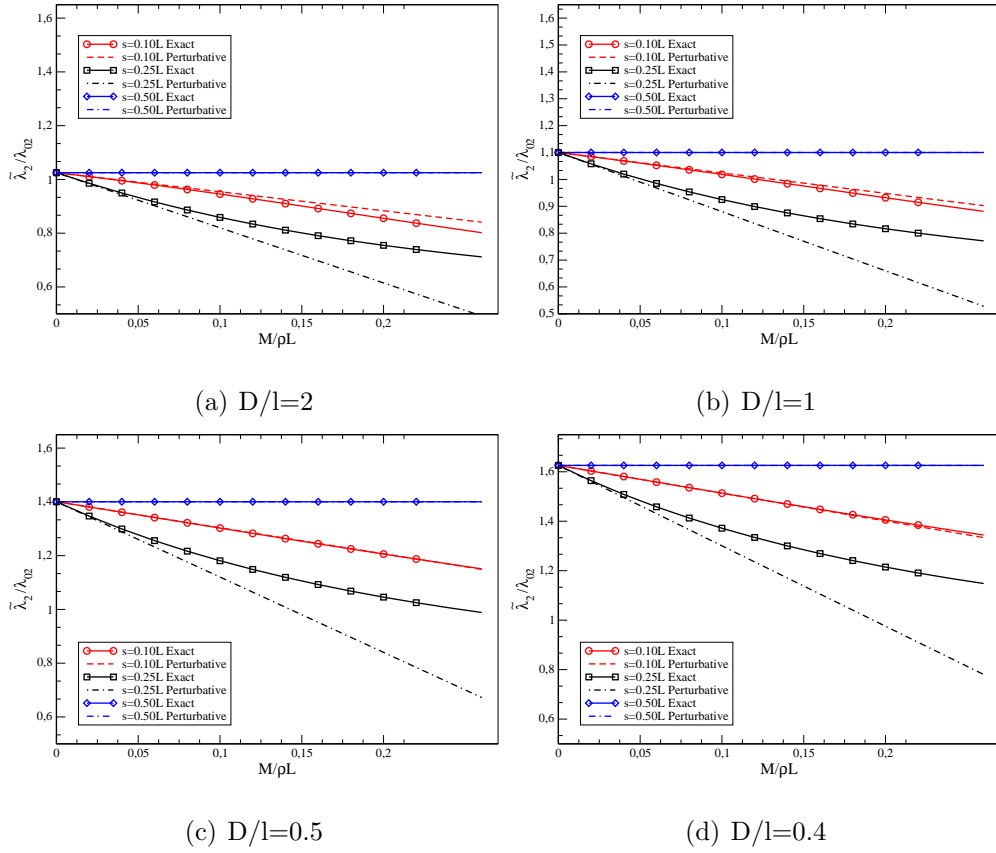


Figure 3: Clamped-clamped nanorod. Normalized second eigenvalue versus dimensionless point-mass, for different mass positions, and different values of the length scale parameter.

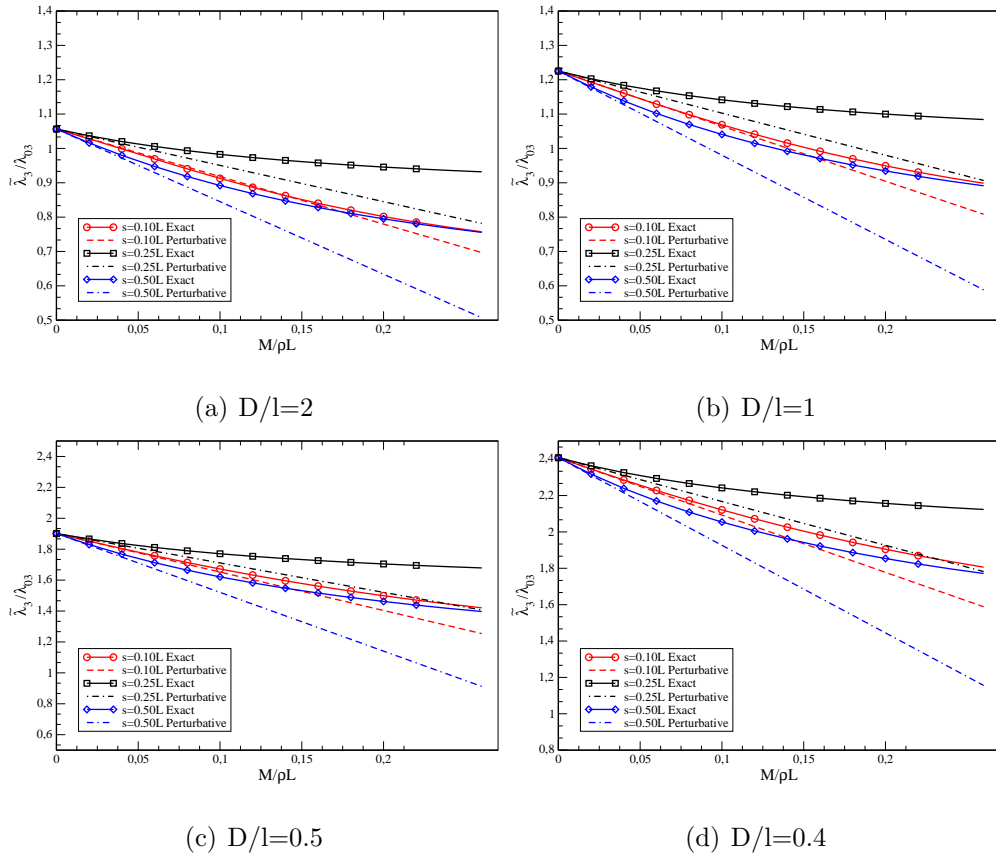


Figure 4: Clamped-clamped nanorod. Normalized third eigenvalue versus dimensionless point-mass, for different mass positions, and different values of the length scale parameter.

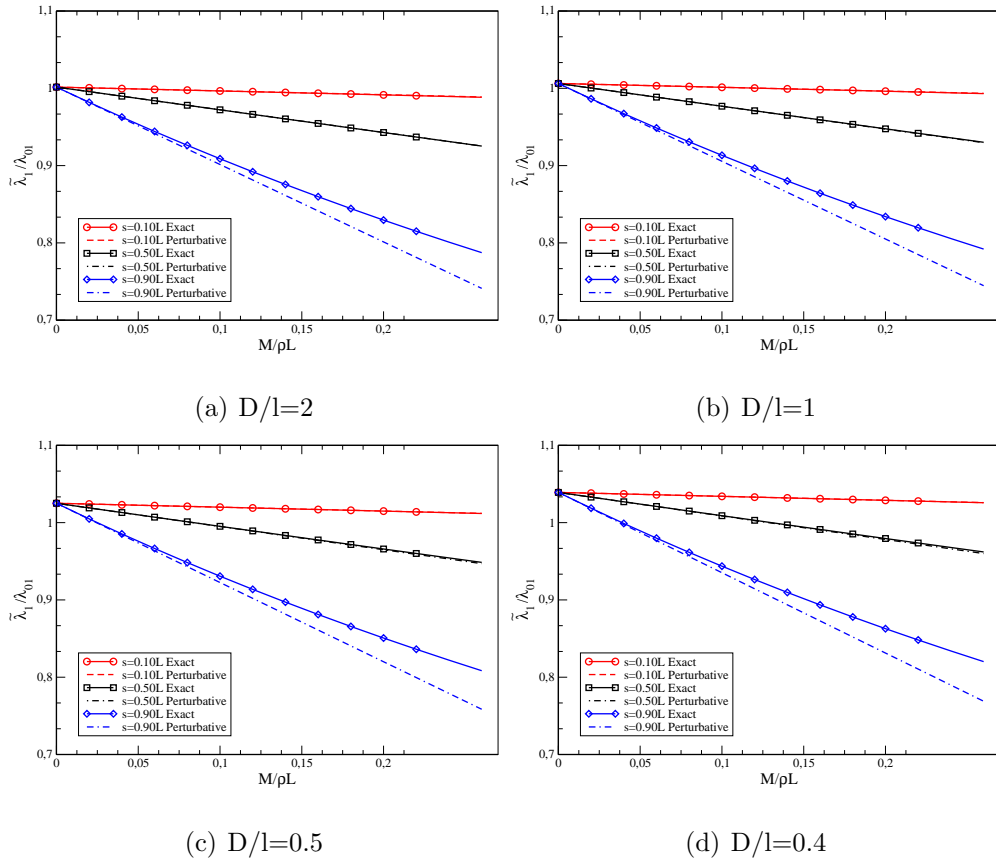


Figure 5: Clamped-free nanorod. Normalized first eigenvalue versus dimensionless point-mass, for different mass positions, and different values of the length scale parameter.

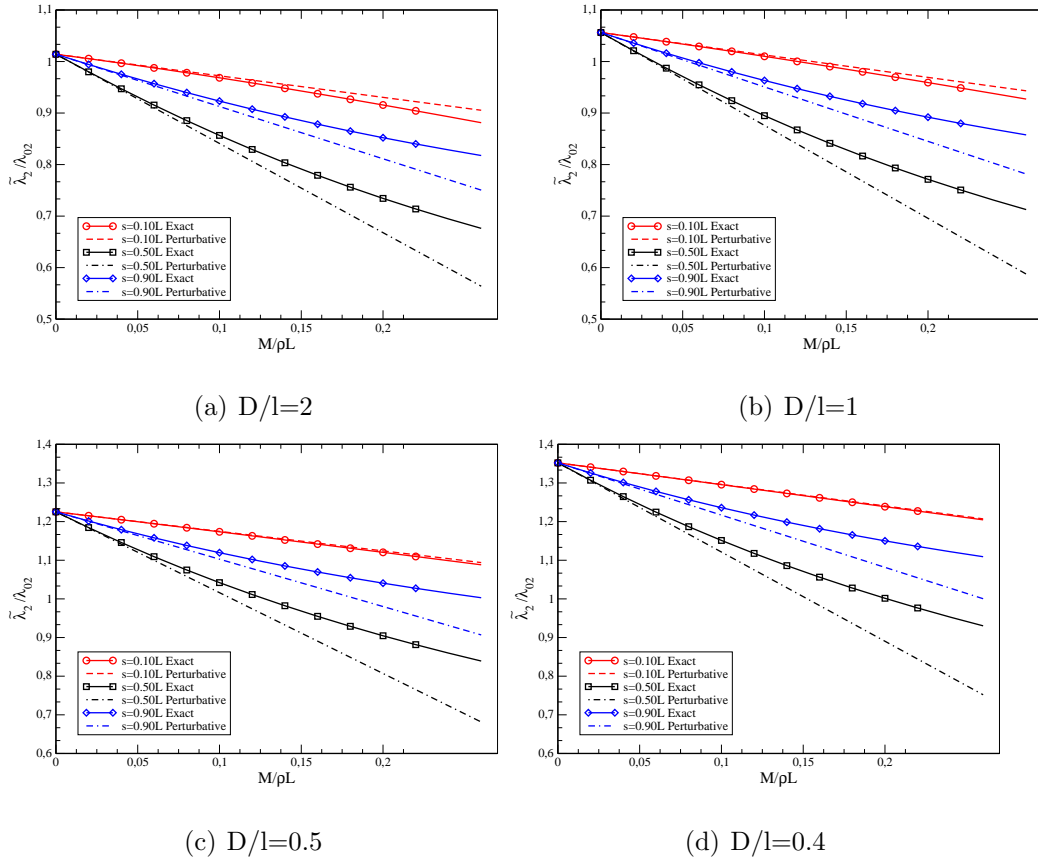


Figure 6: Clamped-free nanorod. Normalized second eigenvalue versus dimensionless point-mass, for different mass positions, and different values of the length scale parameter.

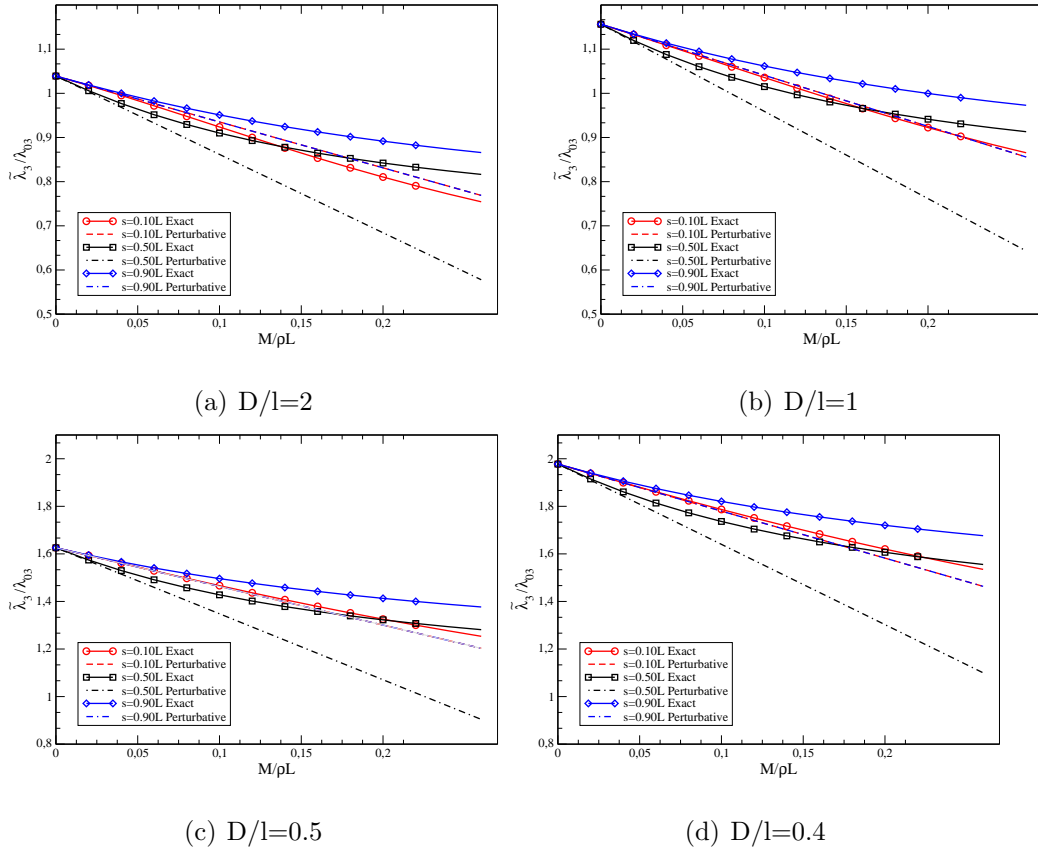


Figure 7: Clamped-free nanorod. Normalized third eigenvalue versus dimensionless point-mass, for different mass positions, and different values of the length scale parameter.

## Highlights

- The vibrations of nanoresonators with a single point mass have been addressed
- The modified strain gradient theory has been used to account for size effects
- Exact and perturbative solutions for the natural frequencies have been obtained
- The point mass identification from minimal frequency data has been considered

# Resonator-based detection in nanorods

A. Morassi<sup>a</sup>, J. Fernández-Sáez<sup>b,\*</sup>, R. Zaera<sup>b</sup>, J.A. Loya<sup>b</sup>

<sup>a</sup>*Polytechnic Department of Engineering and Architecture, University of Udine, via  
Cotonificio 114, 33100 Udine, Italy*

<sup>b</sup>*Department of Continuum Mechanics and Structural Analysis, Universidad Carlos III  
de Madrid, Av. de la Universidad 30, 28911 Leganés, Madrid, Spain*

---

## Abstract

In this paper the axial vibrational behaviour of nanorods with an attached point-mass is studied, using the modified strain energy theory. The natural frequencies of the nanorod with the concentrated mass are obtained for different boundary conditions. The effects of the concentrated mass intensity, mass location, as well as the value of scale parameters have been analysed. For the case of small intensity of the concentrated mass, the natural frequencies of the nanorod can be estimated using a first order perturbative solution. These approximate results are compared with those corresponding to the exact solution. For this case, from the properties of the eigenvalue perturbative theory, the identification of single point mass in uniform nanorods (mass intensity and position) is addressed. The results obtained encourage the use of axial vibrations of nanorods as a very precise sensing technique.

## *Keywords:*

Strain gradient theory, nanorods, nanosensors, mass identification, inverse

---

\*Corresponding author. E-mail address: jose.fernandez@uc3m.es

problems.

---

## 1. Introduction

Nowadays, the scientific community interest is attracted by the use of nanostructures (carbon nanotubes, *CNTs*, graphene sheets, *GSs*, and nanowires) as nano-sensors. The reason is connected with the promising features regarding a wide range of applications such as gas detection, early disease detection, gene mutation detection, DNA sequencing. In this respect, several reviews have been recently published showing the different capabilities of the nanostructures [1, 2, 3]. According to Khanna [4], nano-sensors can be classified into six groups: mechanical, electrical, optical, magnetic, chemical, and thermal.

In this research we are interested in mechanical nanoresonator sensors and, in particular, in vibration based-methods as identification techniques. The sensing principle for this class of nanoresonators is based on the measurement of the variations of the resonant frequencies caused by (unknown) additional masses located on the initial system. The conventional detection principle assumes that the mass perturbation, caused by attachments of foreign atoms or molecules, chemical/molecular adsorption, the presence of virus particles or protein-protein and protein-DNA interactions, can be described as Dirac-delta point masses, having unknown intensities and locations, superimposed to the given mass density of the nanoresonator. We refer to [1] and [5] for more sophisticated mechanical models in which a simultaneous perturbation of the stiffness properties coupled with the mass increase is also

considered in the analysis. Our main goals in the present research are: (i) to derive a continuum mechanical model able to describe the axial vibration of a nanoresonator with a single additional point mass, and (ii) to develop a method for the identification of the point mass from minimal eigenfrequency data. In particular, we shall consider the inverse problem in which the added mass is *small* with respect to the total mass of the nanosensor.

It is well known that the size effects are significant regarding the mechanical behavior of the nanostructures which composes the nanoresonators. The large computational effort required for the Molecular Dynamics techniques (*MD*), see, among others, [6, 7, 8, 9], encourages the exploration of other possibilities, such as generalized continuum mechanics approaches given that classical continuum mechanics cannot predict the size effect, due to its scale-free character.

Among the generalized continuum theories, we cite here three main groups: Cosserat micropolar elasticity [10], the strain gradient elasticity of Mindlin [11, 12], and the nonlocal continuum mechanics initiated by Eringen and coworkers [13, 14], and formulated originally in integral form.

From the early integral nonlocal theory, Eringen [15] introduced a differential constitutive theory showing that, for a specific class of kernel functions, the non-local integral constitutive equation can be transformed into a differential form, much easier to manage than the integral model. From the pioneer work of Peddieson et al. [16], this differential version of the Eringen nonlocal model has been widely used to address the mechanical behaviour (static and dynamic) of nano-structures. The list of papers related with these applica-

tions is extremely long to be reported here. The interested reader can read the very recent review by Rafii-Tabar et al. [17].

Several authors used the Eringen elasticity theory to assess the vibrational behaviour of beams and rods with attached masses. Thus, Elthaer et al. [18], Murmu et al. [19], and Li et al. [20] applied this theory to obtain the shift of the natural frequency of bending vibrations of nanobeams carrying attached mass. Moreover, Murmu et al. [19] and Li et al. [20] provided identification formulas from the approximated expressions of the frequency shift. However, the cases studied in the above papers are rather specific and correspond to a nano-cantilever with a mass attached at the tip or a distributed mass through a certain length from the tip [19], while three configurations, corresponding to a cantilever beam with a mass attached at the tip, simply supported, and bi-clamped beams with the mass attached at the mid-section, are analysed in [20].

Regarding the use of the Eringen elasticity theory applied to *CNTs* with a single attached mass vibrating in axial direction, it is worth to note the work by Aydogdu and Filiz [21] who analyzed the frequencies of axially vibrating *CNTs* (clamped-clamped and clamped-free) with a single attached mass located at different positions.

Li et al. [22] studied the natural frequencies of an axially vibrating nanorod with an elastically restrained end by a nanospring (depending of the stiffness of the nanospring this end could be considered clamped or free), and with an attached mass at the other end considered free. In this analysis, the Love hypotheses are considered (i.e. the inertial effects of radial motion

have been taken into account).

Nevertheless, several authors have pointed out some inconsistencies arising from the Eringen differential model when it is applied to the static behavior of bars in tension [23], static bending behaviour of a Euler-Bernoulli beams [16, 24, 25, 26, 27] or flexural vibrations of a cantilever beam [28].

Recently, Fernández-Sáez et al. [29] and Romano et al. [30] give some new insights on the origin of these inconsistencies. Therefore, a more suitable approach to describe the mechanical behaviour of the nanostructures is needed.

The modified strain gradient elasticity theory was proposed by Lam et al. [31] based on previous developments by Mindlin [12] and Fleck and Hutchinson [32]. This approach needs new additional equilibrium equations to govern the behavior of higher-order stresses, and contain only three non-classical constants for isotropic linear elastic materials. Some papers can be cited to illustrate (the list is not exhaustive) the use of this theory to model the mechanical behaviour of 1D simple nanostructures (beams and rods). Thus, using this approach the static and dynamic bending behavior of Euler-Bernoulli beams [33] and Timoshenko beams has been studied [34]. Akgoz and Civalek [35, 36] obtained analytical solutions for the buckling problem of axially loaded nano-sized beams. The free torsional vibrations of microbars have been analyzed in [37, 38]. Akgoz and Civalek also studied the longitudinal vibrations of homogeneous [39] and nonhomogeneous (functionally graded material) [40] microbars using the simple rod theory, while Guven [41] analyzed the propagation of longitudinal stress waves based on

Love-Bishop hypothesis, i.e. considering the lateral deformation and the shear strain effects.

To our knowledge, there is no theoretical investigation on the axial vibrations of nanorods with attached concentrated mass when the modified strain gradient elasticity theory of Lam et al. [31] is used as constitutive model. This analysis is relevant regarding the nanosensor applications of this kind of structures.

Regarding the experimental determination of frequencies in axially vibrating nanorods, some papers can be found in the literature (see for instance, [42, 43, 44]). However, to the authors knowledge, no experimental works dealing with axially vibrating nanorods with attached masses have been published.

In this paper we analyze the axial vibrational behavior of a nanorod carrying a concentrated mass through its span and subjected to different boundary conditions. The mechanical behavior of the nanorod is modelled using the modified strain gradient theory proposed by Lam et al. [31]. The effects of the mass intensity, location as well as the value of scale parameter have been analyzed. For the case of small intensity of the concentrated mass, a first order perturbative technique is used to estimate the natural frequencies of the nanorod. The approximate results are compared with those corresponding to the exact solution. Basing on the explicit expression of the first-order eigenfrequency change induced by the point mass, we are able to formulate and solve the inverse problem consisting in the identification of the location and intensity of the point mass in a uniform nanorod from

minimal eigenfrequency data. In particular, for nanorods under a specified set of end conditions, the method gives closed-form expressions of both the location and the intensity of the point mass in terms of a suitable pair of eigenfrequencies of the nanorod.

The paper is organized as follows. The mechanical model of the nanorod under longitudinal free vibration with and without point mass is briefly recalled in Section 2. Section 3 is devoted to the illustration of the perturbation effects of the small added mass on the eigenvalues of the nanorod. The inverse problem of identifying the position and the intensity of the small point mass from eigenfrequency shifts is addressed in Section 4. Applications and results of numerical simulations, both of the direct and the inverse eigenvalue problem, are reported and commented in Section 5.

## 2. The mechanical model

### 2.1. Brief resume of the modified strain gradient theory

The modified strain gradient theory was presented by Lam et al. [31], who considered the following expression for the strain energy  $\mathcal{W}$  corresponding to a linear elastic isotropic material occupying a volume  $V$

$$\mathcal{W} = \int_V \left( \sigma_{ij} \varepsilon_{ij} + p_i \gamma_i + \tau_{ijk}^{(1)} \eta_{ijk}^{(1)} + m_{ij}^s \chi_{ij}^s \right) dv, \quad (1)$$

where the notational convention that repeated indices are implicitly summed from 1 to 3 has been adopted hereinafter. Classical and higher order stress

measures  $\sigma_{ij}$ ,  $p_i$ ,  $\tau_{ijk}^{(1)}$ ,  $m_{ij}^s$  are defined as [31]

$$\sigma_{ij} = \left( K - \frac{2G}{3} \right) \delta_{ij} \varepsilon_{mm} + 2G \varepsilon_{ij}, \quad (2)$$

$$p_i = 2Gl_0^2 \gamma_i, \quad (3)$$

$$\tau_{ijk}^{(1)} = 2Gl_1^2 \eta_{ijk}^{(1)}, \quad (4)$$

$$m_{ij}^s = 2Gl_2^2 \chi_{ij}^s, \quad (5)$$

where the strain tensor  $\varepsilon_{ij}$ , the dilatational gradient vector  $\gamma_i$ , the deviatoric stretch gradient tensor  $\eta_{ijk}^{(1)}$  and the symmetric rotation gradient tensor  $\chi_{ij}^s$  are given by

$$\varepsilon_{ik} = \frac{1}{2} (u_{i,j} + u_{j,i}), \quad (6)$$

$$\gamma_i = \varepsilon_{mm,i}, \quad (7)$$

$$\eta_{ijk}^{(1)} = \frac{1}{3} (\varepsilon_{jk,i} + \varepsilon_{ki,j} + \varepsilon_{ij,k}) - \frac{1}{15} [\delta_{ij} (\varepsilon_{mm,k} + 2\varepsilon_{mk,m}) + \delta_{jk} (\varepsilon_{mm,i} + 2\varepsilon_{mi,m}) + \delta_{ki} (\varepsilon_{mm,j} + 2\varepsilon_{mj,m})], \quad (8)$$

$$\chi_{ij}^s = \frac{1}{2} (\theta_{i,j} + \theta_{j,i}). \quad (9)$$

Here,  $u_i$  is the  $i$ th cartesian component of the displacement vector,  $i = 1, 2, 3$ , and  $\theta_i$  is the rotation vector expressed as

$$\theta_i = \frac{1}{2} e_{ijk} u_{k,j}. \quad (10)$$

$\delta_{ij}$  is the Kronecker delta, and  $e_{ijk}$  is the permutation symbol.

Bulk modulus  $K = E/(3(1 - 2\nu))$ ,  $K > 0$ , and shear modulus  $G = E/(2(1 + \nu))$ ,  $G > 0$ , are defined in the classical way in terms of the Young's

modulus  $E$ ,  $E > 0$ , and Poisson ratio  $\nu$ ,  $\nu > 0$ . To complete the model, three additional materials constants,  $l_0 > 0$ ,  $l_1 > 0$ ,  $l_2 > 0$ , which account for scale effects are needed.

## 2.2. Modified strain gradient model for the axial vibrations of a uniform nanorod

Let us specialize the general modified strain gradient theory to the free longitudinal undamped vibrations of a slender straight uniform nanorod of length  $L$ , vibrating along its longitudinal axis  $x$ . Assuming the hypothesis of the simple theory of thin bars (i.e., rigid translation of the cross section along the  $x$  direction), the equation governing the axial displacement  $U(x, t)$  of the nanorod reads as, see [39] for details,

$$aU''(x, t) - bU^{IV}(x, t) = \rho\ddot{U}(x, t), \quad (11)$$

where  $U'(x, t)$  and  $\dot{U}(x, t)$  indicate the first partial derivative of the function  $U$  with respect to  $x$  and  $t$ , respectively,  $x \in (0, L)$  and  $t > 0$ .

According to [39], the coefficient  $a$ ,  $a > 0$ , plays the role of the axial stiffness of the nanorod, and it can be conventionally expressed as  $a = EA$ . Here,  $A$  is a geometrical parameter, which, in analogy with classical large-scale rods, can be made coincident with the cross-sectional area of the nanorod. The coefficient  $\rho > 0$  is the constant mass per unit length. The coefficient  $b$  takes the expression

$$b = GA \left( 2l_0^2 + \frac{4}{5}l_1^2 \right). \quad (12)$$

Using the classical separation of variables method, the axial displacement  $U(x, t)$  can be expressed as

$$U(x, t) = u(x)e^{i\omega t}, \quad (13)$$

where  $u = u(x)$  is the amplitude of the normal mode (eigenfunction) associated to the natural (radian) frequency  $\omega$ . Substituting Eq.(13) into Eq.(11), the following ordinary differential equation is obtained

$$bu^{IV} - au'' = \lambda\rho u, \quad x \in (0, L), \quad (14)$$

$\lambda = \omega^2$  being the eigenvalue. We shall be concerned with the following sets of classical (left) and non-classical (right) boundary conditions.

#### **Clamped-Clamped (C-C)**

$$u(0) = 0, \quad u''(0) = 0, \quad (15)$$

$$u(L) = 0, \quad u''(L) = 0; \quad (16)$$

#### **Clamped-Free (C-F)**

$$u(0) = 0, \quad u''(0) = 0, \quad (17)$$

$$u'(L) = 0, \quad u'''(L) = 0; \quad (18)$$

#### **Free-Free (F-F)**

$$u'(0) = 0, \quad u'''(0) = 0, \quad (19)$$

$$u'(L) = 0, \quad u'''(L) = 0. \quad (20)$$

The non-classical end conditions selected above are only one of the possible sets of non-classical boundary conditions that may be assigned at the ends of a nanorod. Our choice is motivated by the fact that these boundary operators ensure the self-adjointness of the eigenvalue problem and, then, the reality of the eigenvalues. To show this, let  $\mathcal{D} = \left(b \frac{d^4}{dx^4} - a \frac{d^2}{dx^2}\right)$  be the nanorod operator in (14) and let us denote by  $\mathcal{B}$  a boundary operator either of the type  $(C - C)$ ,  $(C_F)$  or  $(F_F)$ , e.g., in case  $(C - C)$ ,  $\mathcal{B}u = 0$  means  $u(0) = u''(0) = 0 = u(L) = u''(L)$ . A direct calculation shows that  $\int_0^L (\mathcal{D}u)v = \int_0^L u(\mathcal{D}v)$  for every  $u, v \in C^4(0, L)$  for which  $\mathcal{B}u = \mathcal{B}v = 0$ , that is the pair  $\{\mathcal{D}, \mathcal{B}\}$  is self-adjoint.

The following properties of the eigenvalue problem (14), coupled with one of the boundary conditions (15)–(16), (17)–(18), (19)–(20) can be deduced from the general theory:

i) there exists an infinite sequence of real non-negative eigenvalues  $\{\lambda_n\}_{n=1}^\infty$ , with  $\lim_{n \rightarrow \infty} \lambda_n = \infty$ , all of which are simple.

ii) The family of the eigenfunctions  $\{u_n(x)\}_{n=1}^\infty$  is an orthogonal basis of the space of the admissible deformations of the nanorod.

iii) The  $n$ th eigenvalue of the nanorod differential equation (14), coupled with one set of boundary conditions of the type  $(C - C)$ ,  $(C - F)$  or  $(F - F)$ , is greater than the  $n$ th eigenvalue of the corresponding classical rod. The inequality is always strict, with the exception of the first (vanishing) eigenvalue of the case  $(F - F)$ . This property was already noticed in the literature (see, for example, Figure 5 and Figure 6 in [39]), and it is a consequence of the extremum properties of the eigenvalues [45]. The property follows by

noticing that an admissible deformation of the nanorod is also an admissible deformation of the classical rod, and that the strain energy density of the nanorod is bigger than the strain energy density of the classical rod, see the variational characterization of the eigenvalues given in (35)–(37) below.

Moreover, a direct inspection of the eigenvalue problem shows that if  $v$  is an eigenfunction of the classical rod (satisfying the differential equation (14) with  $b = 0$  and one set of classical boundary conditions of the type  $(C - C)$ ,  $(C - F)$  or  $(F - F)$ ), then  $v$  is also an eigenfunction of the nanorod under the same set of (classical and non-classical) end conditions; and vice versa.

The above general properties can be easily confirmed by the direct determination of the following closed form expressions of the eigenpairs of (14) coupled with one of the three boundary conditions  $(C - C)$ ,  $(C - F)$ ,  $(F - F)$ .

### Clamped-Clamped (C-C)

$$u_n^{C-C}(x) = \sqrt{\frac{2}{\rho L}} \sin\left(\frac{n\pi x}{L}\right), \quad (21)$$

$$\lambda_n^{C-C} = \left(\frac{n\pi}{L}\right)^2 \left[ \frac{1}{\rho} \left( a + b \left(\frac{n\pi}{L}\right)^2 \right) \right], \quad n \geq 1; \quad (22)$$

### Clamped-Free (C-F)

$$u_n^{C-F}(x) = \sqrt{\frac{2}{\rho L}} \sin\left(\frac{(2n-1)\pi x}{2L}\right), \quad (23)$$

$$\lambda_n^{C-F} = \left(\frac{(2n-1)\pi}{2L}\right)^2 \left[ \frac{1}{\rho} \left( a + b \left(\frac{(2n-1)\pi}{2L}\right)^2 \right) \right], \quad n \geq 1; \quad (24)$$

### Free-Free (F-F)

$$u_n^{F-F}(x) = \sqrt{\frac{2}{\rho L}} \cos\left(\frac{n\pi x}{L}\right), \quad (25)$$

$$\lambda_n^{F-F} = \left(\frac{n\pi}{L}\right)^2 \left[ \frac{1}{\rho} \left( a + b \left(\frac{n\pi}{L}\right)^2 \right) \right], \quad n \geq 0. \quad (26)$$

According to Eqs. (11) and (12),  $l_2$  does not play any role in the equation governing the axial displacement. Thus, the only material constants accounting for length scale effects are  $l_0$  and  $l_1$ , which are grouped in the parameter  $b$ . From the Eqs. (22), (24) and (26) it can be easily shown that increasing values of  $l_0$  or  $l_1$  leads to higher values of the natural frequencies.

#### 2.3. Free axial vibrations of a uniform nanorod carrying a point mass

Basing on the conventional detection principle (see the Introduction), we assume that a point mass  $M$  is added at the cross-section of the nanorod of abscissa  $s$ ,  $s \in (0, L)$ , see Fig. 1. The differential operator governing the eigenvalue problem for the nanorod with a point mass is

$$b\tilde{u}^{IV} - a\tilde{u}'' = \tilde{\lambda}\rho\tilde{u}, \quad x \in (0, s) \cup (s, L), \quad (27)$$

where, in addition to one of the end conditions (15)–(16), (17)–(18), (19)–(20), we have also to consider the jump conditions at  $x = s$

$$\left\{ \begin{array}{l} [[\tilde{u}(s)]] = 0, \end{array} \right. \quad (28)$$

$$\left\{ \begin{array}{l} [[\tilde{u}'(s)]] = 0, \end{array} \right. \quad (29)$$

$$\left\{ \begin{array}{l} [[\tilde{u}''(s)]] = 0, \end{array} \right. \quad (30)$$

$$\left\{ \begin{array}{l} [[(a\tilde{u}' - b\tilde{u}''')(s)]] = -\tilde{\lambda}M\tilde{u}(s), \end{array} \right. \quad (31)$$

where  $[[\varphi(s)]] = (\varphi(s^+) - \varphi(s^-))$  denotes the jump of the function  $\varphi$  at  $x = s$ . The unperturbed nanorod clearly corresponds to  $M \rightarrow 0^+$ .

To solve the eigenvalue problem for the nanorod with a point mass we need to find a nontrivial  $\tilde{u} \in C^4((0, s) \cup (s, L)) \cap C^1((0, L))$  and  $\tilde{\lambda} \in \mathbb{R}^+$  such that (27)–(31) are satisfied, under a given set of end conditions.

In the sequel, we shall need the weak formulation of the eigenvalue problem. Let  $H^m(a, b)$ , with  $-\infty < a < b < +\infty$ , be the real-valued Hilbert space of the Lebesgue measurable functions  $f : (a, b) \rightarrow \mathbb{R}$  such that  $\int_a^b \left( f^2 + \sum_{i=1}^m \left( \frac{d^i f}{dx^i} \right)^2 \right) < +\infty$ , where  $\frac{d^i f}{dx^i}$  is the  $i$ th weak derivative of  $f$ . For the sake of simplicity, we shall consider the specific case of boundary conditions  $(C - C)$ . The other cases  $(C - F)$  and  $(F - F)$  can be managed similarly.

Let us multiply (27) by  $\varphi \in H^2((0, s) \cup (s, L))$  satisfying  $[[\varphi(s)]] = [[\varphi'(s)]] = 0$  and end conditions  $\varphi(0) = 0 = \varphi(L)$ . Integrating by parts twice, we have

$$\begin{aligned} b\tilde{u}'''\varphi \Big|_0^{s^-} + b\tilde{u}'''\varphi \Big|_{s^+}^L - b\tilde{u}''\varphi' \Big|_0^{s^-} - b\tilde{u}''\varphi' \Big|_{s^+}^L - a\tilde{u}'\varphi \Big|_0^{s^-} - a\tilde{u}'\varphi \Big|_{s^+}^L + \\ + \int_0^L (b\tilde{u}''\varphi'' + a\tilde{u}'\varphi') = \tilde{\lambda} \int_0^L \rho\tilde{u}\varphi \end{aligned} \quad (32)$$

Using the jump and end conditions on  $\tilde{u}$  at  $x = s$  and  $x = 0, L$ , respectively, and by the definition of  $\varphi$ , we get the weak formulation of (27)–(31) under  $(C - C)$  boundary conditions: to find  $\tilde{u} \in \mathcal{H} \setminus (0)$  and  $\tilde{\lambda} \in \mathbb{R}$  such that

$$\int_0^L (b\tilde{u}''\varphi'' + a\tilde{u}'\varphi') = \tilde{\lambda} \left( M\tilde{u}(s)\varphi(s) + \int_0^L \rho\tilde{u}\varphi \right), \quad \text{for every } \varphi \in \mathcal{H}, \quad (33)$$

where

$$\mathcal{H} = \{f : (0, L) \rightarrow \mathbb{R} \mid f \in H^2((0, s) \cup (s, L)), f(0) = 0 = f(L), [[f(s)]] = [[f'(s)]] = 0\}. \quad (34)$$

The Rayleigh's quotient  $R[\cdot]$  associated to the weak formulation (33)–(34) is

$$R : \mathcal{H} \setminus \{0\} \rightarrow \mathbb{R}^+, \quad R[\varphi] = \frac{\int_0^L b(\varphi'')^2 + a(\varphi')^2}{M\varphi^2(s) + \int_0^L \rho\varphi^2} \quad (35)$$

and the  $n$ th eigenpair  $(\tilde{\lambda}_n, \tilde{u}_n(x))$  is such that

$$\tilde{\lambda}_n = \min_{\varphi \in \mathcal{V}_n \setminus \{0\}} R[\varphi] = R[\tilde{u}_n], \quad n \geq 1, \quad (36)$$

where

$$\mathcal{V}_n = \left\{ f \in \mathcal{H} \mid Mf(s)\tilde{u}_i(s) + \int_0^L \rho f\tilde{u}_i dx = 0, \quad i = 1, \dots, n-1 \right\}. \quad (37)$$

It can be shown that properties i) and ii) mentioned above for the unperturbed nanorod apply also to the eigenvalue problem for the nanorod carrying a point mass. However, closed-form solutions for the eigenpairs are generally not available, even for the constant coefficient case.

### 3. Eigenvalue shifts induced by a small point mass: a perturbative approach

In this section we shall assume that the point mass  $M$  is small with respect to the total mass of the nanorod, i.e.,

$$M \ll \rho L. \quad (38)$$

Under this assumption, we shall investigate on the effects of the added mass on the eigenvalues of the nanorod. Again, to simplify the presentation, attention is focused on  $(C - C)$  end conditions. From the variational theory of eigenvalues recalled in (35)–(37), it easily follows that no natural frequency can be increased due to the addition of the point mass  $M$ , i.e.,

$$\tilde{\lambda}_n \leq \lambda_n, \quad \text{for every } n \geq 1. \quad (39)$$

However, in order to study the inverse problem of identifying the point mass by natural frequency data, we need quantitative information on the effects of the added mass. A first result is contained in the next statement.

**Proposition 3.1.** *Let  $(\tilde{\lambda}, \tilde{u})$  be an eigenpair of (33)–(34). Then, for a given position  $s \in (0, L)$  of the point mass,  $\tilde{\lambda} = \tilde{\lambda}(M)$  is a  $C^1$ -function in  $(0, \infty)$  and we have*

$$\frac{\partial \tilde{\lambda}}{\partial M} = -\tilde{\lambda} \frac{\tilde{u}^2(s)}{M\tilde{u}^2(s) + \int_0^L \rho \tilde{u}^2} \quad (40)$$

*Proof.* We apply to the weak formulation (33) the forward-difference operator

$$\delta_h f(x; M) = \frac{f(x; M+h) - f(x; M)}{h}, \quad h > 0, \quad M \in (0, \infty). \quad (41)$$

We have

$$\begin{aligned} \int_0^L (b(\delta_h \tilde{u}'') \varphi'' + a(\delta_h \tilde{u}') \varphi') &= \delta_h \tilde{\lambda} \left( M \tilde{u}(s) \varphi(s) + \int_0^L \rho \tilde{u} \varphi \right) + \\ &\tilde{\lambda} \left[ \tilde{u}(s) \varphi(s) + M (\delta_h \tilde{u}(s)) \varphi(s) + \int_0^L \rho (\delta_h \tilde{u}) \varphi \right], \end{aligned} \quad (42)$$

for every  $C^2$ -piecewise function  $\varphi$  in  $[0, L]$ , with  $\varphi(0) = 0 = \varphi(L)$ .

Let us take  $\varphi = \tilde{u}$  and let us note that  $\delta_h \tilde{u}$  is a suitable test function for the weak formulation of the problem. Then

$$\int_0^L (b(\delta_h \tilde{u}'') \tilde{u}'' + a(\delta_h \tilde{u}') \tilde{u}') = \delta_h \tilde{\lambda} \left( M \tilde{u}^2(s) + \int_0^L \rho \tilde{u}^2 \right) + \tilde{\lambda} \tilde{u}^2(s) + \tilde{\lambda} \left[ M(\delta_h \tilde{u}(s)) \tilde{u}(s) + \int_0^L \rho(\delta_h \tilde{u}) \tilde{u} \right] \quad (43)$$

The left hand side of (43) simplifies with the last square bracket on the right end side. Then, taking the limit as  $h \rightarrow 0^+$ , we obtain

$$\frac{\partial \tilde{\lambda}}{\partial M}(M^+) = -\tilde{\lambda} \frac{\tilde{u}^2(s)}{M \tilde{u}^2(s) + \int_0^L \rho \tilde{u}^2}. \quad (44)$$

By repeating the above analysis with the backward-difference operator  $\delta_{-h}(\cdot)$ , the left derivative of the eigenvalue  $\tilde{\lambda} = \tilde{\lambda}(M)$  turns out to be equal to the right derivative. Then, the function  $\tilde{\lambda} = \tilde{\lambda}(M)$  is continuously differentiable and (40) is proved.  $\square$

By adapting the arguments in [46], we can prove the following useful result.

**Theorem 3.2.** *There exists  $\widehat{M}, \widetilde{M} > 0$ , such that the eigenvalues  $\tilde{\lambda}_n = \tilde{\lambda}_n(M)$  of (33)–(34) are holomorphic functions of  $M$ , for  $0 < M < \widehat{M}$ .*

By Proposition 3.1 and Theorem 3.2, and assuming the mass-normalization condition  $\int_0^L \rho u_n^2 = 1$ , the Taylor series expansion truncated to the first order term in the smallness parameter  $M$  for the  $n$ th eigenvalue is given by

$$\tilde{\lambda}_n(M) = \lambda_n - \lambda_n u_n^2(s) M. \quad (45)$$

Relation (45) shows that the change in an eigenvalue can be written as the product of the eigenvalue itself, the square of the corresponding (mass-normalized) eigenfunction of the unperturbed nanorod evaluated at the mass position, and the mass variation. Equation (45) plays an important role in our inverse problem, since it shows that the ratios of the relative changes in two different eigenvalues depend only on the location of the point mass, not on its magnitude, namely (if  $\delta\lambda_k < 0$ )

$$\frac{\frac{\delta\lambda_n}{\lambda_n}}{\frac{\delta\lambda_k}{\lambda_k}} = \frac{u_n^2(s)}{u_k^2(s)} \equiv f(s), \quad (46)$$

where  $\delta\lambda_n \equiv \tilde{\lambda}_n - \lambda_n$  and  $s \in (0, L)$ . Note that if  $\delta\lambda_k = 0$ , then the possible point mass location coincides with one of the node points of the  $k$ th vibrating mode  $u_k$  of the unperturbed nanorod. Therefore, the problem of localizing the point mass is reduced to the determination of the solutions of (46) for fixed/measured value of the ratio  $\frac{\delta\lambda_n}{\lambda_n} / \frac{\delta\lambda_k}{\lambda_k}$ . Let us observe that, once the unperturbed configuration is known, the function  $f = f(s)$  can be determined numerically or analytically. This idea was first explored in [47] for the identification of a point mass in a full-scale longitudinally vibrating rod under free-free end conditions, see also [48]. It should be noticed that the analysis developed in [47] and [48] deals with the identification of a point mass, described as a Dirac's delta, in a classical *second-order* Sturm-Liouville operator, whereas, as it was shown in Section 2, the longitudinal vibration of a nanorod involves a *fourth-order* differential operator.

In the next section we shall show that there are certain situations in which a suitable choice of the frequency input data allows obtaining closed

form solutions of the linearized inverse problem.

#### 4. Identification of a small point mass in uniform nanorods

We first consider the identification of the small point mass  $M$  in a nanorod under clamped-clamped end conditions ( $C - C$ ). Recalling the expressions of the eigenpairs (25)–(26), by (45) we have

$$C_n^{C-C} = M \sin^2 \left( \frac{n\pi s}{L} \right), \quad (47)$$

where

$$C_n^{C-C} = -\frac{\left( \tilde{\lambda}_n^{C-C} - \lambda_n^{C-C} \right) \rho L}{\lambda_n^{C-C}} \frac{\rho L}{2}, \quad n \geq 1. \quad (48)$$

A direct calculation shows that

$$M \left( 4C_n^{C-C} - C_{2n}^{C-C} \right) = 4 \left( C_n^{C-C} \right)^2, \quad n \geq 1. \quad (49)$$

In order to identify the point mass, let us distinguish two cases.

*First case.* Let us assume  $C_n^{C-C} > 0$  (note that  $C_1^{C-C}$  is always strictly positive). By equation (49) we have

$$M = \frac{C_n^{C-C}}{1 - \frac{C_{2n}^{C-C}}{4C_n^{C-C}}}, \quad (50)$$

which gives a closed-form expression for the mass intensity  $M$  in terms of the ( $n$ th,  $2n$ th) eigenfrequency changes. It is worth noticing that, by (49),  $M$  in (50) takes positive values. The position of the point mass can be determined by inserting the expression (50) into (47), namely

$$S = \cos \left( \frac{2n\pi s}{L} \right) = \frac{C_{2n}^{C-C}}{2C_n^{C-C}} - 1, \quad (51)$$

where  $S \in [-1, 1]$ . By taking  $n = 1$  in (51), the ratio of the first frequency changes is sufficient for the localization of the point mass, up to a symmetrical position with respect to the mid-point of the nanorod.

*Second case.* If  $C_n^{C-C} = 0$  for certain  $n \geq 2$ , then from (47) we have  $S = 1$ , that is the point mass is located in one of the points of zero-sensitivity of the  $n$ th vibration mode.

The above analysis shows that the pair of natural frequencies  $n$ th and  $2n$ th plays a special role in the linearized inverse problem. In fact, if the  $n$ th frequency is sensitive to the point mass, that is  $C_n^{C-C} > 0$  or equivalently  $u_n^2(s) > 0$ , then the pair  $\{C_n^{C-C}, C_{2n}^{C-C}\}$  determines uniquely the mass intensity  $M$ . It is worth noticing that the expression for  $M$  is the same for all the pairs of values  $\{C_n^{C-C}, C_{2n}^{C-C}\}$ . Concerning the possible point mass locations, equation (51) shows that their number generally increases as the order  $n$  of the frequencies involved increases, which accounts for the recourse to "low" frequencies for solving the localization problem.

Summing up, we have shown that the measurement of the first two natural frequencies in a clamped-clamped nanorod allows for the unique identification of the point mass (except for symmetrical positions). This conclusion must be modified for nanorods under different boundary conditions. As an example, let us consider the identification of the point mass in a clamped free nanorod from the first and second eigenfrequency changes. By inserting the expressions (23)–(24) into (45) we have

$$C_1^{C-F} = M \sin^2\left(\frac{\pi s}{2L}\right), \quad C_2^{C-F} = M \sin^2\left(\frac{3\pi s}{2L}\right). \quad (52)$$

Let  $z = \cos\left(\frac{\pi s}{L}\right)$ , with  $z \in (-1, 1)$ . Then, recalling the identity  $\cos(3\alpha) = (4\cos^3\alpha - 3\cos\alpha)$ , we obtain the following non-linear system in terms of the two unknowns  $z$  and  $M$

$$\begin{cases} C_1^{C-F} = \frac{M}{2}(1 - z), & (53) \\ C_2^{C-F} = \frac{M}{2}(1 - 4z^3 + 3z). & (54) \end{cases}$$

A direct calculation shows that

$$(9C_1^{C-F} - C_2^{C-F}) = 2M(z - 1)^2(z + 2) > 0 \quad (55)$$

and the damage localization problem (46) for  $n = 2$  and  $k = 1$  is reduced to solving the polynomial equation

$$(1 + 2z)^2 = \chi, \quad z \in (-1, 1), \quad (56)$$

where, by (55),

$$\chi = \frac{C_2^{C-F}}{C_1^{C-F}} \in [0, 9]. \quad (57)$$

The existence and the number of solutions of (56) depend on the values of the parameter  $\chi$ . If  $\chi \in [1, 9)$ , then there exists a unique solution  $z_1 \in (0, 1)$ , which corresponds to  $s_1 \in (0, \frac{L}{2})$ . If  $\chi \in (0, 1)$ , then there are two distinct solutions of (56), say  $z_1 \in (-1, -\frac{1}{2})$  and  $z_2 \in (-\frac{1}{2}, 0)$ , which correspond to  $s_1 \in (\frac{2L}{3}, L)$  and  $s_2 \in (\frac{L}{2}, \frac{2L}{3})$ , respectively. Finally, for  $\chi = 0$  equation (56) has a double zero at  $z = -\frac{1}{2}$ , corresponding to  $s = \frac{2L}{3}$ . In conclusion, should the point mass be located within the left half of the rod adjacent to the clamped end, the measurement of the first and second natural frequencies determines uniquely the location of the point mass. Conversely, should the

mass be located in the right half of the rod, there are two different locations corresponding to the same value  $\chi$ , apart when  $\chi = 0$ , which corresponds to the mass position at  $s = \frac{2}{3}L$ .

We conclude this section with the analysis of natural frequency data coming from two sets of different end conditions. It turns out that the measurement of the  $n$ th resonant frequency under boundary conditions  $(C - C)$  and the  $n$ th natural frequency under boundary conditions  $(F - F)$ ,  $n \geq 1$ , determines uniquely the point mass and the location variable  $S = \cos\left(\frac{2m\pi s}{L}\right)$ . In particular, by adopting the above procedure, we have

$$M = C_n^{F-F} + C_n^{C-C} \quad (58)$$

and

$$\text{if } C_n^{F-F} > 0, \quad \text{then } S = -1 + \frac{2}{1 + \frac{C_n^{C-C}}{C_n^{F-F}}}; \quad (59)$$

$$\text{if } C_n^{F-F} = 0, \quad \text{then } S = -1. \quad (60)$$

Here,  $C_n^{F-F} = -\frac{(\tilde{\lambda}_n^{F-F} - \lambda_n^{F-F})}{\lambda_n^{F-F} \frac{2}{\rho L}}$ ,  $n \geq 1$ . It follows that the point mass is uniquely determined (except for symmetrical positions) by  $\{C_1^{C-C}, C_1^{F-F}\}$ .

## 5. Applications

### 5.1. Exact versus perturbative solution

This section is devoted to the evaluation of the accuracy of the perturbation approach outlined in Section 3 in estimating the eigenvalues of the problem (27)–(31) with boundary conditions given either by (15)–(16)  $(C - C)$  or by (17)–(18)  $(C - F)$ . From the practical point of view, the free-free case

$(F - F)$  does not seem to be very suitable for nanosensors applications, and will not be considered in the sequel.

Following [39], we considered a nanorod with circular cross-section with diameter  $D$  and length  $L = 20D$ . Moreover, the two scale parameters  $l_0$  and  $l_1$  have been assumed to be equal, e.g.,  $l_0 = l_1 = l$ , and the selected Poisson's ratio was  $\nu = 0.38$ . The variation of the first three eigenvalues,  $\tilde{\lambda}_1, \tilde{\lambda}_2, \tilde{\lambda}_3$  (normalized to the corresponding eigenvalues  $\lambda_{0n}$  of the "classical" local rod, that is the rod with  $b = 0$ , without any attached mass) with respect to the intensity  $M$  of the point mass (normalized to the total mass of the nanorod  $\rho L$ ) has been calculated for various positions  $s$  and for  $D/l = \{2.0, 1.0, 0.5, 0.4\}$ .

Eigenfrequency changes have been obtained using both exact and perturbative solutions. The exact solution is calculated from the corresponding frequency equation in terms of nondimensional eigenvalue  $\Lambda = \frac{\rho L^2}{EA} \tilde{\lambda}$ , and nondimensional attached mass  $\bar{M} = \frac{M}{\rho L}$ .

For the case of a clamped-clamped nanorod the frequency equation reads as

$$f^{C-C}(\Lambda) = -\beta \sinh(\beta) \left( \alpha h^2 (\alpha^2 + \beta^2) \sin(\alpha) - \Lambda \bar{M} \sin(\alpha s) \sin(\alpha(1-s)) \right) - \alpha \Lambda \bar{M} \sin(\alpha) \sinh(s\beta) \sinh(\beta(1-s)) = 0, \quad (61)$$

where the parameters  $\alpha$  and  $\beta$  are given by

$$\alpha = \sqrt{\frac{\sqrt{4h^2\Lambda + 1} - 1}{2h^2}}, \quad (62)$$

$$\beta = \sqrt{\frac{\sqrt{4h^2\Lambda + 1} + 1}{2h^2}}, \quad (63)$$

and  $h$  is the dimensionless parameter related to the length scale  $l$  by the following expression:

$$h = \sqrt{\frac{7}{5(1+\nu)}} \frac{l}{20D}. \quad (64)$$

The frequency equation for the clamped-free nanorod is

$$\begin{aligned} f^{C-F}(\Lambda) = \beta \cosh(\beta) (\alpha h^2 (\alpha^2 + \beta^2) \cos(\alpha) - \Lambda \bar{M} \sin(\alpha s) \cos(\alpha(1-s)) + \\ + \alpha \Lambda \bar{M} \cos(\alpha) \sinh(s\beta) \cosh(\beta(1-s\beta))) = 0. \end{aligned} \quad (65)$$

The first order change in eigenvalues is determined from (45), where  $u_n$  and  $\lambda_n$  are given by (21)–(22) and (23)–(24) for  $(C-C)$  and  $(C-F)$  end conditions, respectively.

Figs. 2 to 4 show, for the  $(C-C)$  boundary conditions, the variation of the first three eigenvalues with the attached mass located at different positions and for the selected values of  $D/l$ . For moderate values of the attached mass, i.e.  $M/\rho L \in [0, 0.2]$ , there is a good agreement between exact and first-order solution. For the fundamental mode, for example, the accuracy generally decreases as the mass location moves toward the mid-point of the nanorod. In fact, the maximum difference is encountered at  $s = \frac{L}{2}$ , and it

oscillates between 15 and 22 percent. As it was observed above, in absence of the attached mass, eigenfrequency values of the strain gradient nanorod are higher than those of the classical rod model, and they increase when the scale parameter  $l$  increases ( $D/l$  decreases), meaning that the generalized constitutive model used leads to a stiffening of the structure.

The results corresponding to clamped-free boundary conditions are shown in Figs. 5 to 7, and considerations analogous to the clamped-clamped case can be made. In the case of the fundamental mode, the maximum difference between exact and perturbative results occurs for mass location  $s = 0.9$ , and its value is about 16 percent.

### *5.2. Solution of the inverse problem*

In this section some results on the capability of the method proposed in Section 4 to identify the value of the attached mass and its position are presented. For the clamped-clamped nanorod, among several simulations, the cases with mass intensity  $M/(\rho L) \in \{0.001, 0.025, 0.050, 0.100, 0.200\}$  and position  $s/L \in \{0.1, 0.25, 0.40, 0.50\}$  shall be considered in detail. It should be noticed that positions  $s/L > 1/2$  are not considered given the symmetry of the problem. The attached mass is identified using equations (48) and (50), while the position is obtained from equation (51). Table 1 collects the results when the first two natural frequencies are used in the identification process, i.e., for  $n = 1$ . It can be seen that, for small masses, the error in the identification of position and mass intensity remains at relatively small values. The case  $s/L = 0.50$  deserves special attention, since the position

is exactly identified. Larger errors are observed when the mass intensity increases.

Similar information is given in Table 2, in which the second and fourth frequencies are used (i.e.,  $n = 2$ ). Besides the fact that two possible solutions for the mass position can exist, the comparison of the values with those given in Table 1 shows that the precision in the identification of position and mass decreases, even for the identified location closest to the right one (except when  $s = 0.25$ , for which the method gives the exact solution). Specifically, for  $s = 0.5$  the identification method leads to imaginary values since this position coincides with a node of both the second and fourth shape modes, thus both the second and the fourth frequencies are insensitive to the presence of the point mass.

In the case of the clamped-free rod, as explained in the second part of Section 4, a different scenario is found. The method was tested for the same point mass intensities considered in the previous case, and the positions investigated covered the whole span of the rod, namely  $s = \{0.10, 0.35, 0.50, 0.65, 0.90\}$ , since the symmetry conditions do not hold for the clamped-free case. The mass location has been determined by solving (56). In agreement with the theory (e.g., case in which  $s \in (0, \frac{L}{2})$ ), for  $s = 0.10$  and  $s = 0.35$  only one solution is encountered in the identification process (see Table 3). The errors are moderate and increase with the attached mass intensity. For the other positions considered in simulations, two possible solutions are obtained,  $Sln.1$  and  $Sln.2$  (see Table 4), which correspond to  $s_1 \in (\frac{2L}{3}, L)$ , and  $s_2 \in (\frac{L}{2}, \frac{2L}{3})$ , respectively. In every case, as expected from the theory developed in the sec-

ond part of Section 4, one of these two solutions is close to the true solution, the other is spurious and follows from the non-uniqueness of the mathematical inverse problem. In all the cases, the mass intensity  $M$  was estimated by solving (55). It should be noticed that, for the sake of brevity, all the results quoted correspond to  $D/l = 0.4$ , the higher value of the scale parameter  $l$  considered in this study.

In order to evaluate the effect of errors on the data measurements, the 1st and 2nd eigenfrequencies were perturbed for a clamped-clamped nanorod ( $C - C$ ) with point mass intensity  $M/\rho L = 0.025$  at  $s = 0.4L$ , according to the expressions

$$\sqrt{\tilde{\lambda}_1^{pert}} = \sqrt{\tilde{\lambda}_1} (1 + \tau_1); \quad \sqrt{\tilde{\lambda}_2^{pert}} = \sqrt{\tilde{\lambda}_2} (1 + \tau_2) , \quad (66)$$

where  $\tau_1$  and  $\tau_2$  are real random Gaussian variables with zero mean and standard deviations  $\sigma_1$  and  $\sigma_2$ , respectively. The maximum measurement error has been taken to be approximately equal to a given percentage  $\Pi$ ,  $\Pi = 5, 10, 15, 20\%$  of the frequency shift  $\delta\lambda_n$ , for  $n = 1, 2$ . Then, the standard deviations are defined as  $3\sigma_n = \delta\lambda_n\Pi/100$ , for  $n = 1, 2$ . A MonteCarlo simulation on a population of 10000 samples was performed, leading to the results presented in Table 5, where the mean and standard deviations for the identification errors corresponding to mass intensity and position are shown for different values of the measurement error  $\Pi$ . As it can be seen, the mean errors keep (approximately) constant with  $\Pi$ , and equal to the corresponding identification errors shown in Table 1. Regarding the standard deviation, it increases with the measurement error, but keeps at a rather low value up to

$\mathit{II} = 0.20$ . All this confirms the robustness of the proposed method.

## 6. Concluding remarks

In this paper we obtained the natural frequencies of the axial vibrations of a nanorod carrying a concentrated mass through its span for both clamped-clamped and clamped-free end conditions. The modified strain gradient theory proposed in [31] has been used to take into account the size effects present in this kind of structures. The influence of the mass intensity, mass location, as well as the value of scale parameter have been analysed. For the case of small intensity of the concentrated mass, a first order perturbative technique is used to compute the natural frequencies of the nanorod. To our knowledge, this problem, which is relevant regarding application of nanostructures as sensors, is addressed for the first time. In fact, from the properties of the eigenvalue perturbative theory, the identification of a single point mass in a uniform nanorod (mass intensity and position) by minimal frequency data has been considered. We have shown that the point mass can be uniquely identified (up to a symmetrical position) by the knowledge of the first two natural frequencies of the nanorod under clamped-clamped end conditions. Moreover, the effect of the frequency measurement errors on the estimated variables (mass intensity and location) has been illustrated with a statistical analysis, showing the robustness of the identification method. The results obtained herein encourage the use of axial vibrations of nanorods as a very precise sensing technique.

As a final remark, we point out that a problem worth of investigation that

emerges from the present analysis stands on the possibility of identifying a point mass of finite - not necessarily small - magnitude. It is likely that the results and methods presented in [49, 50] may be useful for this purpose.

### **Acknowledgement**

The authors wish to acknowledge *Ministerio de Economía y Competitividad de España* for the financial support, under grant number DPI2014-57989-P. The first author also gratefully acknowledges the financial support of the National Research Project PRIN2015 'Identificazione e diagnostica di sistemi strutturali complessi'.

## References

## References

- [1] K. Eom, H. S. Park, D. S. Yoon, T. Kwon, Nanomechanical resonators and their applications in biological/chemical detection: Nanomechanics principles, *Physics Reports* 503 (2011) 115–163.
- [2] Q. Wang, B. Arash, A review on applications of carbon nanotubes and graphenes as nano-resonator sensors, *Computational Materials Science* 82 (2014) 350–360.
- [3] B. Arash, J. W. Jiang, T. Rabczuk, A review on nanomechanical resonators and their applications in sensors and molecular transportation, *Applied Physics Reviews* 2 (2015) 021301.
- [4] V. K. Khanna, *Nanosensors: Physical, Chemical, and Biological*, CRC Press, Boca raton, FL, 2012.
- [5] J. Tamayo, D. Ramos, J. Mertens, M. Calleja, Effect of the adsorbate stiffness on the resonance response of microcantilever sensors, *Applied Physics Letters* 89 (2006) 224104.
- [6] C. Wei, D. Srivastava, Nanomechanics of carbon nanofibers: Structural and elastic properties, *Applied Physics Letters* 85 (2004) 2208—2210.
- [7] X. Q. He, K. M. Liew, C. Wei, Mechanical properties of carbon nanocones, *Applied Physics Letters* 91 (2007) 261906–261906–3.

- [8] K. M. Liew, J. X. Wei, X. Q. He, Carbon nanocones under compression: Buckling and post-buckling behaviors, *Physical Review B- Condensed Matter and Materials Physics* 75 (2007) 195435.
- [9] P. Tsai, T. Fang, A molecular dynamics study of the nucleation, thermal stability and nanomechanics of carbon nanocones, *Nanotechnology* 18 (2007) 105702.
- [10] E. Cosserat, F. Cosserat, *Theory of Deformable Bodies*, (Translated by D.H. Delphenich), Scientific Library, A. Hermann and Sons, Paris, 1909.
- [11] R. D. Mindlin, Micro-structure in linear elasticity, *Archive for Rational Mechanics and Analysis* 16 (1964) 51–78.
- [12] R. D. Mindlin, Second gradient of strain and surface-tension in linear elasticity, *International Journal of Solids and Structures* 1 (1965) 417–438.
- [13] A. C. Eringen, Linear theory of nonlocal elasticity and dispersion of plane-waves, *International Journal of Engineering Science* 10 (5) (1972) 233–248.
- [14] A. C. Eringen, D. G. B. Edelen, Nonlocal elasticity, *International Journal of Engineering Science* 10 (3) (1972) 233–248.
- [15] A. C. Eringen, On differential-equations of nonlocal elasticity and solutions of screw dislocation and surface-waves, *Journal of Applied Physics* 54 (9) (1983) 4703–4710.

- [16] J. Peddieson, G. R. Buchanan, R. P. McNitt, Application of nonlocal continuum models to nanotechnology, *International Journal of Engineering Science* 41 (3-5) (2003) 305–312.
- [17] H. Rafii-Tabar, E. Ghavanloo, S. A. Fazelzadeh, Nonlocal continuum-based modeling of mechanical characteristics of nanoscopic structures, *Physics Reports* 638 (2016) 1–97.
- [18] M. A. Eltaher, M. A. Agwa, F. F. Mahmoud, Nanobeam sensor for measuring a zeptogram mass, *International Journal of Mechanics and Materials in Design* 12 (2016) 211–221.
- [19] T. Murmu, S. Adhikari, Nonlocal frequency analysis of nanoscale biosensors, *Sensors and Actuators A: Physical* 173 (2012) 41–48.
- [20] X. F. Li, G. J. Tang, Z. B. Shen, K. Lee, Resonance frequency and mass identification of zeptogram-scale nanosensor based on the nonlocal beam theory, *Ultrasonics* 55 (2015) 75–84.
- [21] M. Aydogdu, S. Filiz, Modeling carbon nanotube-based mass sensors using axial vibration and nonlocal elasticity, *Physica E: Low-dimensional Systems and Nanostructures* 43 (2011) 1229–1234.
- [22] X. F. Li, G. J. Tang, Z. B. Shen, K. Y. Lee, Size-dependent resonance frequencies of longitudinal vibration of a nonlocal Love nanobar with a tip nanoparticle, *Mathematics and Mechanics of Solids* (2016) doi: 10.1177/1081286516640597.

- [23] E. Benvenuti, A. Simone, One-dimensional nonlocal and gradient elasticity: Closed-form solution and size effect, *Mechanics Research Communications* 48 (2013) 46–51.
- [24] Q. Wang, K. M. Liew, Application of nonlocal continuum mechanics to static analysis of micro- and nano-structures, *Physics Letters A* 363 (3) (2007) 236–242, wang, Q. Liew, K.M.
- [25] N. Challamel, C. M. Wang, The small length scale effect for a non-local cantilever beam: a paradox solved, *Nanotechnology* 19 (2008) 345703(7).
- [26] C. Wang, S. Kitipornchai, C. Lim, M. Eisenberger, Beam bending solutions based on nonlocal Timoshenko beam theory, *Journal of Engineering Mechanics* 134 (6) (2008) 475–481.
- [27] N. Challamel, Z. Zhang, C. M. Wang, J. N. Reddy, Q. Wang, T. Micheli, B. Collet, On nonconservativeness of Eringen’s nonlocal elasticity in beam mechanics: correction from a discrete-based approach, *Archive of Applied Mechanics* 84 (2014) 1275 – 1292.
- [28] P. Lu, H. P. Lee, C. Lu, P. Q. Zhang, Dynamic properties of flexural beams using a nonlocal elasticity model, *Journal of Applied Physics* 99 (2006) 1 – 9.
- [29] J. Fernández-Sáez, R. Zaera, J. A. Loya, J. N. Reddy, Bending of Euler-Bernoulli beams using Eringen’s integral formulation: A paradox resolved, *International Journal of Engineering Science* 99 (2016) 107–116.

- [30] G. Romano, R. Barretta, M. Diaco, F. Marotti de Sciarra, Constitutive boundary conditions and paradoxes in nonlocal elastic nanobeams, *International Journal of Mechanical Sciences* 121 (2017) 151–156.
- [31] D. C. C. Lam, F. Yang, A. C. M. Chong, J. Wang, P. Tong, Experiments and theory in strain gradient elasticity, *Journal of the Mechanics and Physics of Solids* 51 (2003) 1477–1508.
- [32] N. A. Fleck, J. W. Hutchinson, Strain gradient plasticity, *Advances in Applied Mechanics* 33 (1997) 295–361.
- [33] S. Kong, S. Zhou, Z. Nie, K. Wang, Static and dynamic analysis of micro-beams based on strain gradient elasticity theory, *International Journal of Engineering Science* 47 (2009) 487–498.
- [34] B. Wang, J. Zhao, S. Zhou, A microscale Timoshenko beam model based on strain gradient elasticity theory, *European Journal of Mechanics A-Solids* 29 (2010) 837–843.
- [35] B. Akgoz, O. Civalek, Strain gradient elasticity and modified couple stress models for buckling analysis of axially loaded micro-scaled beams, *International Journal of Engineering Science* 49 (2011) 1268–1280.
- [36] B. Akgoz, O. Civalek, A new trigonometric beam model for buckling of strain gradient microbeams, *International Journal of Mechanical Sciences* 81 (2014) 88–94.

- [37] M. Kahrobaiyan, S. Tajalli, M. Movahhedy, J. Akbari, M. Ahmadian, Torsion of strain gradient bars, *International Journal of Engineering Science* 49 (2011) 856–866.
- [38] S. Narendar, S. Gopalakrishnan, Strain gradient torsional vibration analysis of micro/nano rods, *International Journal of Nano Dimension* 3 (2012) 1–17.
- [39] B. Akgoz, O. Civalek, Longitudinal vibration analysis for microbars based on strain gradient elasticity theory, *Journal of Vibration and Control* 20 (2014) 606–616.
- [40] B. Akgoz, O. Civalek, Longitudinal vibration analysis of strain gradient bars made of functionally graded materials(FGM), *Composites: Part B* 55 (2013) 263–268.
- [41] U. Guven, Love-Bishop rod solution based on strain gradient elasticity theory, *Comptes Rendus Mecanique* 342 (2014) 8–16.
- [42] K. Yu, P. Zijlstra, J. E. Sader, Q.-H. Xu, M. Orrit, Damping of Acoustic Vibrations of Immobilized Single Gold Nanorods in Different Environments, *Nano Letters* 13 (6) (2013) 2710–2716.
- [43] M. A. Mahmoud, D. O’Neil, M. A. El-Sayed, Shape- and Symmetry-Dependent Mechanical Properties of Metallic Gold and Silver on the Nanoscale, *Nano Letters* 14 (2) (2014) 743–748.

- [44] P. Guo, R. D. Schaller, L. E. Ocola, J. B. Ketterson, R. P. H. Chang, Gigahertz Acoustic Vibrations of Elastically Anisotropic Indium-Tin-Oxide Nanorod Arrays, *Nano Letters* 16 (9) (2016) 5639–5646.
- [45] R. Courant, D. Hilbert, *Methods of Mathematical Physics*, (first English edition) ed., Interscience Publishers Inc., New York, 1966.
- [46] T. Kato, *Perturbation Theory for Linear Operators*, Springer, Berlin, Germany, 1995.
- [47] A. Morassi, M. Dilena, On point mass identification in rods and beams from minimal frequency measurements, *Inverse Problems in Engineering* 10 (2002) 183–201.
- [48] A. Akhtyamov, A. Ayupova, Point mass identification in rods, *Russian Journal of Nondestructive Testing* 49 (2013) 572–578.
- [49] L. Rubio, J. Fernandez-Saez, A. Morassi, Crack identification in non-uniform rods by two frequency data, *International Journal of Solids and Structures* 75-76 (2015) 61–80.
- [50] J. Fernandez-Saez, A. Morassi, M. Pressacco, L. Rubio, Unique determination of a single crack in a uniform simply supported beam in bending vibration, *Journal of Sound and Vibration* 371 (2016) 94–109.

## Table Captions

Table 1. Identification of the mass intensity  $M$  and position  $s$  in a clamped-clamped nanorod ( $C - C$ ) from the first and second natural frequencies.  $D/l = 0.4$ . Percentage errors:  $e_s = 100 \times (s_{est} - s)/s$ ,  $e_M = 100 \times (M_{est} - M)/M$ .

Table 2. Identification of the mass intensity  $M$  and position  $s$  in a clamped-clamped nanorod ( $C - C$ ) from the second and fourth natural frequencies.  $D/l = 0.4$ . Existence of two solutions for the mass position ( $e_{s1}$  and  $e_{s2}$ ). Percentage errors:  $e_s = 100 \times (s_{est} - s)/s$ ,  $e_M = 100 \times (M_{est} - M)/M$ . \*: no results.

Table 3. Identification of the mass intensity  $M$  and position  $s$  in a clamped-free nanorod ( $C - C$ ) from the first and second natural frequencies.  $D/l = 0.4$ .  $s \in (0, \frac{L}{2})$ : existence of unique solution. Percentage errors:  $e_s = 100 \times (s_{est} - s)/s$ ,  $e_M = 100 \times (M_{est} - M)/M$ .

Table 4. Identification of the mass intensity  $M$  and position  $s$  in a clamped-free nanorod ( $C - F$ ) from the first and second natural frequencies.  $D/l = 0.4$ .  $s \in [\frac{L}{2}, L]$ : existence of two solutions ( $Sln.1$  and  $Sln.2$ ). Percentage errors:  $e_s = 100 \times (s_{est} - s)/s$ ,  $e_M = 100 \times (M_{est} - M)/M$ .

Table 5. Mean and standard deviation for the errors corresponding to the identification of mass intensity and position from the first and second natural frequencies, as a function of the frequency measurement error. Clamped-clamped nanorod ( $C - C$ ) with  $M/\rho L = 0.025$  and  $s = 0.4L$ .

## Figure Captions

Figure 1. Nanorod with a point mass  $M$  located at abscissa  $s$  under different boundary conditions. (a) Clamped-clamped; (b) clamped-free.

Figure 2. Clamped-clamped nanorod. Normalized first eigenvalue versus dimensionless point-mass, for different mass positions, and different values of the length scale parameter.

Figure 3. Clamped-clamped nanorod. Normalized second eigenvalue versus dimensionless point-mass, for different mass positions, and different values of the length scale parameter.

Figure 4. Clamped-clamped nanorod. Normalized third eigenvalue versus dimensionless point-mass, for different mass positions, and different values of the length scale parameter.

Figure 5. Clamped-free nanorod. Normalized first eigenvalue versus dimensionless point-mass, for different mass positions, and different values of the length scale parameter.

Figure 6. Clamped-free nanorod. Normalized second eigenvalue dimensionless point-mass, for different mass positions, and different values of the length scale parameter.

Figure 7. Clamped-free nanorod. Normalized third eigenvalue dimensionless point-mass, for different mass positions, and different values of the length scale parameter.

Table 1: Identification of the mass intensity  $M$  and position  $s$  in a clamped-clamped nanorod ( $C - C$ ) from the first and second natural frequencies.  $D/l = 0.4$ . Percentage errors:  $e_s = 100 \times (s_{est} - s)/s$ ,  $e_M = 100 \times (M_{est} - M)/M$ .

$\frac{M}{\rho L}$	$s = 0.10L$		$s = 0.25L$		$s = 0.40L$		$s = 0.50L$	
	$e_s$	$e_M$	$e_s$	$e_M$	$e_s$	$e_M$	$e_s$	$e_M$
0.010	0.18	-0.24	1.34	-2.54	0.09	-1.62	0	-1.83
0.025	0.61	-0.91	3.26	-6.04	0.22	-3.97	0	-4.46
0.050	1.72	-2.76	6.21	-11.16	0.42	-7.68	0	-8.56
0.100	5.37	-8.70	11.29	-19.37	0.77	-14.39	0	-15.85
0.200	17.06	-24.74	18.95	-30.85	1.34	-25.49	0	-27.54

Table 2: Identification of the mass intensity  $M$  and position  $s$  in a clamped-clamped nanorod ( $C - C$ ) from the second and fourth natural frequencies.  $D/l = 0.4$ . Existence of two solutions for the mass position ( $e_{s1}$  and  $e_{s2}$ ). Percentage errors:  $e_s = 100 \times (s_{est} - s)/s$ ,  $e_M = 100 \times (M_{est} - M)/M$ . \*: no results.

$\frac{M}{\rho L}$	$s = 0.10L$			$s = 0.25L$			$s = 0.40L$			$s = 0.50L$		
	$e_{s1}$	$e_{s2}$	$e_M$	$e_{s1}$	$e_{s2}$	$e_M$	$e_{s1}$	$e_{s2}$	$e_M$	$e_{s1}, e_{s2}$	$e_M$	
0.010	2.65	297.35	-4.34	0	0	-2.59	-74.38	-0.62	-6.28	*	*	
0.025	6.65	293.35	-10.31	0	0	-6.29	-73.53	-1.47	-14.23	*	*	
0.050	13.19	286.81	-18.78	0	0	-12.00	-72.31	-72.31	-24.62	*	*	
0.100	25.02	274.98	-31.01	0	0	-21.88	-70.43	-70.43	-38.84	*	*	
0.200	42.72	257.28	-44.49	0	0	-36.80	-68.0	-68.01	-54.90	*	*	

Table 3: Identification of the mass intensity  $M$  and position  $s$  in a clamped-free nanorod ( $C - F$ ) from the first and second natural frequencies.  $D/l = 0.4$ .  $s \in (0, \frac{L}{2})$ : existence of unique solution. Percentage errors:  $e_s = 100 \times (s_{est} - s)/s$ ,  $e_M = 100 \times (M_{est} - M)/M$ .

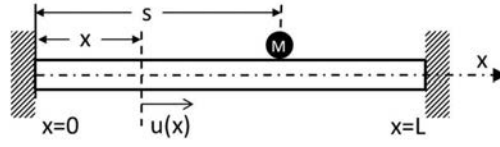
$\frac{M}{\rho L}$	$s = 0.10L$		$s = 0.35L$	
	$e_s$	$e_M$	$e_s$	$e_M$
0.010	-0.68	1.42	0.94	-2.00
0.025	-1.88	3.94	2.29	-4.79
0.050	-3.59	7.72	4.40	-8.97
0.100	-6.18	13.87	8.12	-15.91
0.200	-7.83	18.34	14.05	-26.05

Table 4: Identification of the mass intensity  $M$  and position  $s$  in a clamped-free nanorod ( $C - F$ ) from the first and second natural frequencies.  $D/l = 0.4$ .  $s \in [\frac{l}{2}, L]$ : existence of two solutions ( $Sln.1$  and  $Sln.2$ ). Percentage errors:  $e_s = 100 \times (s_{est} - s)/s$ ,  $e_M = 100 \times (M_{est} - M)/M$ .

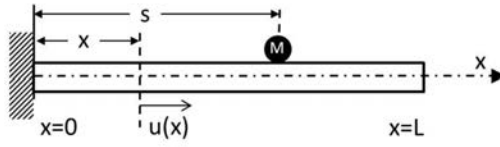
$\frac{M}{\rho L}$	$s = 0.50L$						$s = 0.65L$						$s = 0.90L$					
	$Sln.1$		$Sln.2$		$Sln.1$		$Sln.2$		$Sln.1$		$Sln.2$		$Sln.1$		$Sln.2$			
	$e_s$	$e_M$	$e_s$	$e_M$	$e_s$	$e_M$	$e_s$	$e_M$	$e_s$	$e_M$	$e_s$	$e_M$	$e_s$	$e_M$	$e_s$	$e_M$		
0.010	96.19	-50.39	0.11	-1.04	5.22	-7.26	-0.01	-1.38	-0.38	-1.58	-42.59	82.16						
0.025	94.00	-50.96	0.28	-2.57	5.23	-9.16	-0.02	-3.37	-0.91	-3.87	-42.42	76.67						
0.050	91.59	-51.89	0.55	-5.03	5.24	-12.16	-0.03	-6.53	-1.66	-7.49	-42.16	68.21						
0.100	88.32	-53.67	1.07	-9.64	5.27	-17.63	-0.06	-12.28	-2.84	-14.08	-41.73	53.47						
0.200	84.11	-56.92	1.97	-17.72	5.33	-26.79	-0.11	-21.94	-4.42	-25.02	-41.09	30.48						

Table 5: Mean and standard deviation for the errors corresponding to the identification of mass intensity and position from the first and second natural frequencies, as a function of the frequency measurement error. Clamped-clamped nanorod ( $C-C$ ) with  $M/\rho L = 0.025$  and  $s = 0.4L$ .

Measurement Error, $\Pi$ (%)	Mass mean error (%)	Mass standard dev.	Position mean error (%)	Position standard dev.
5	-3.970	$1.05 \cdot 10^{-4}$	0.217	$2.71 \cdot 10^{-4}$
10	-3.962	$2.09 \cdot 10^{-4}$	0.217	$5.39 \cdot 10^{-4}$
15	-3.957	$3.11 \cdot 10^{-4}$	0.217	$8.10 \cdot 10^{-4}$
20	-3.983	$4.20 \cdot 10^{-4}$	0.211	$10.84 \cdot 10^{-4}$



(a)



(b)

Figure 1: Nanorod with a point mass  $M$  located at abscissa  $s$  under different boundary conditions. (a) Clamped-clamped; (b) clamped-free.

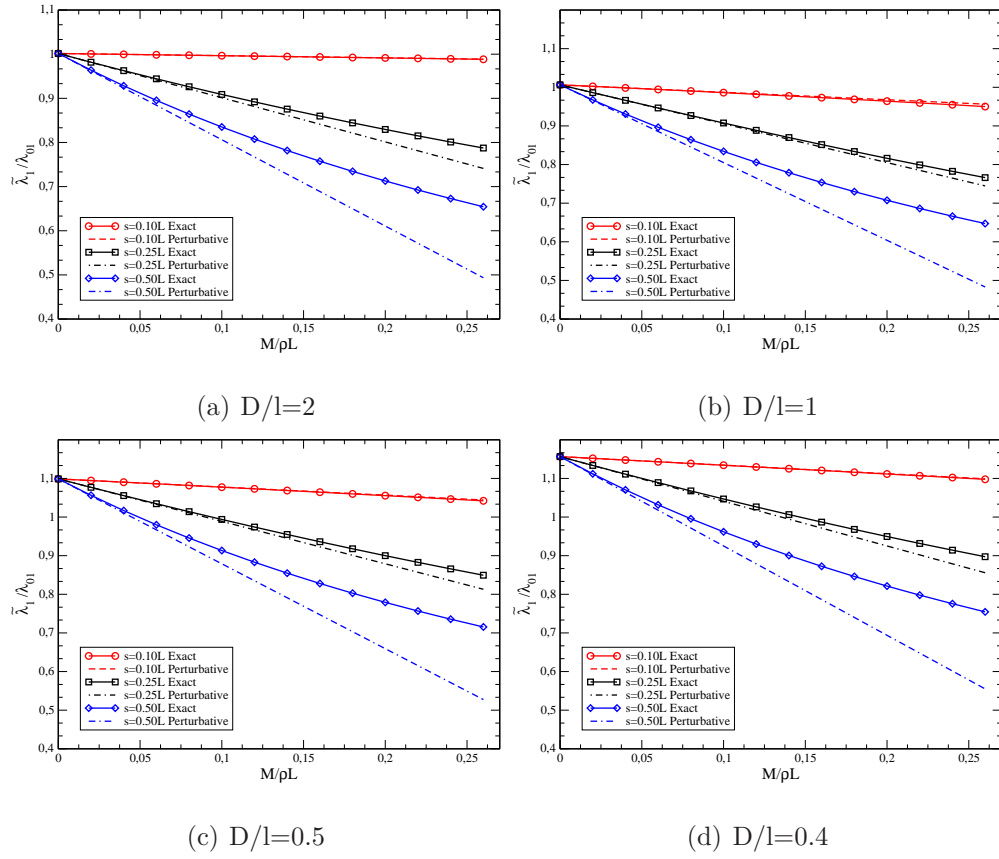


Figure 2: Clamped-clamped nanorod. Normalized first eigenvalue versus dimensionless point-mass, for different mass positions, and different values of the length scale parameter.

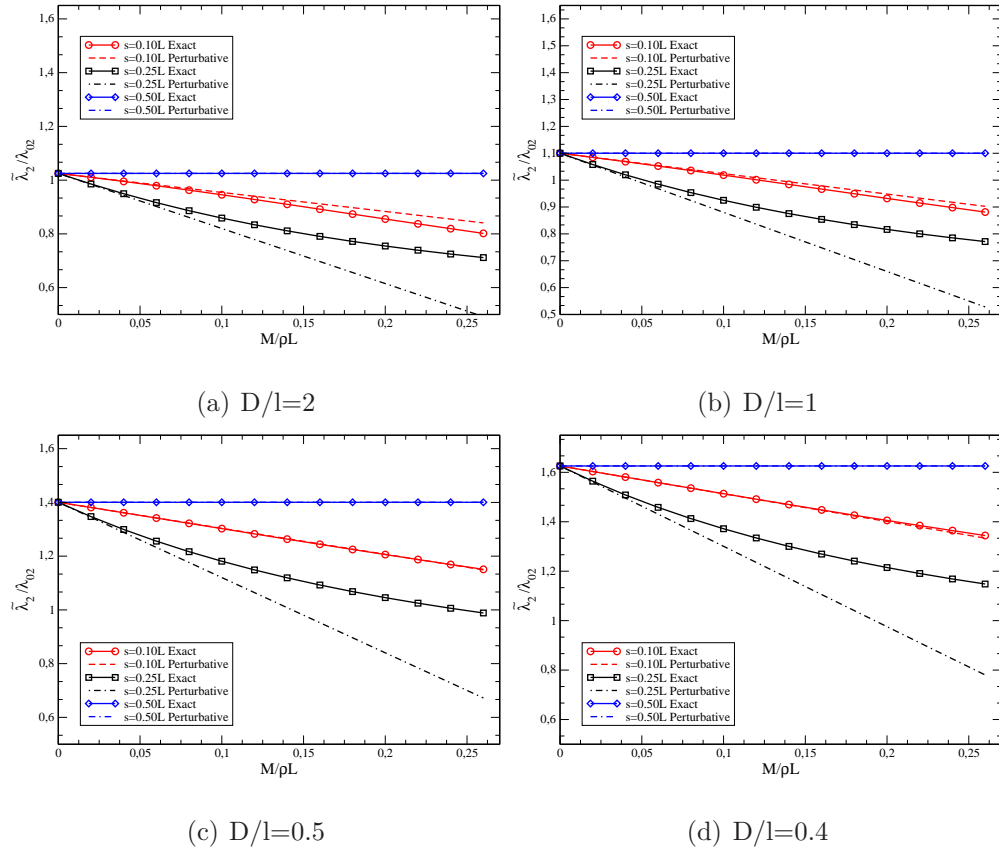


Figure 3: Clamped-clamped nanorod. Normalized second eigenvalue versus dimensionless point-mass, for different mass positions, and different values of the length scale parameter.

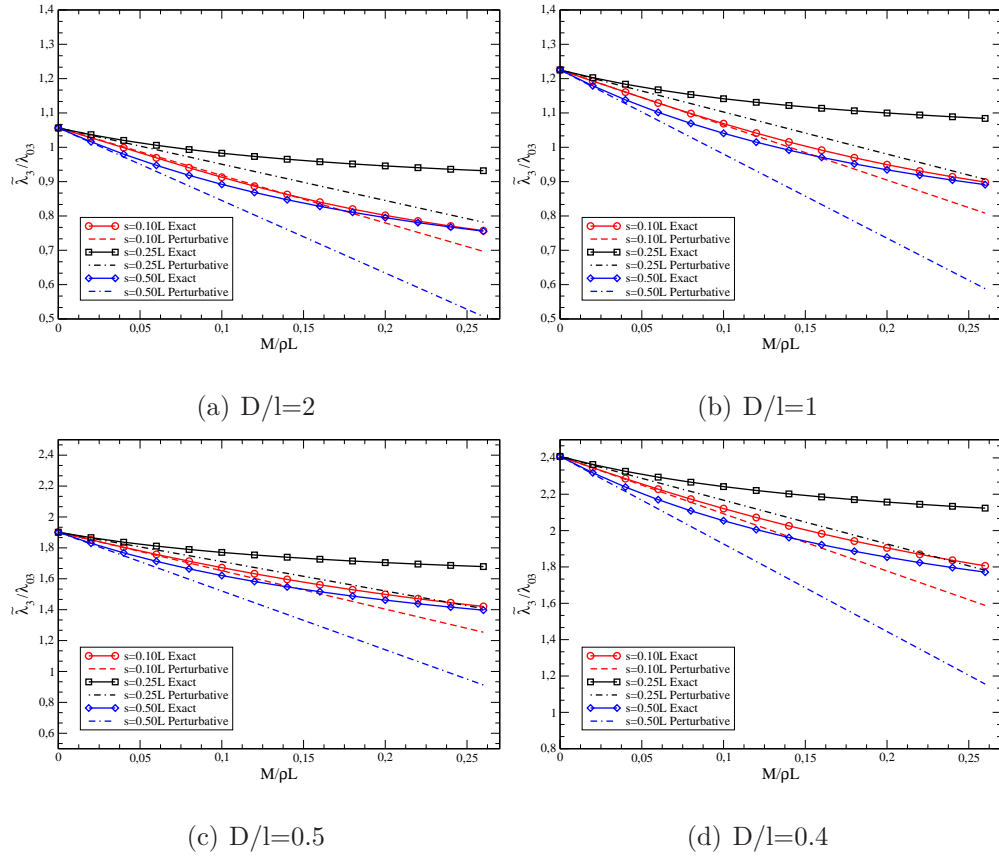


Figure 4: Clamped-clamped nanorod. Normalized third eigenvalue versus dimensionless point-mass, for different mass positions, and different values of the length scale parameter.

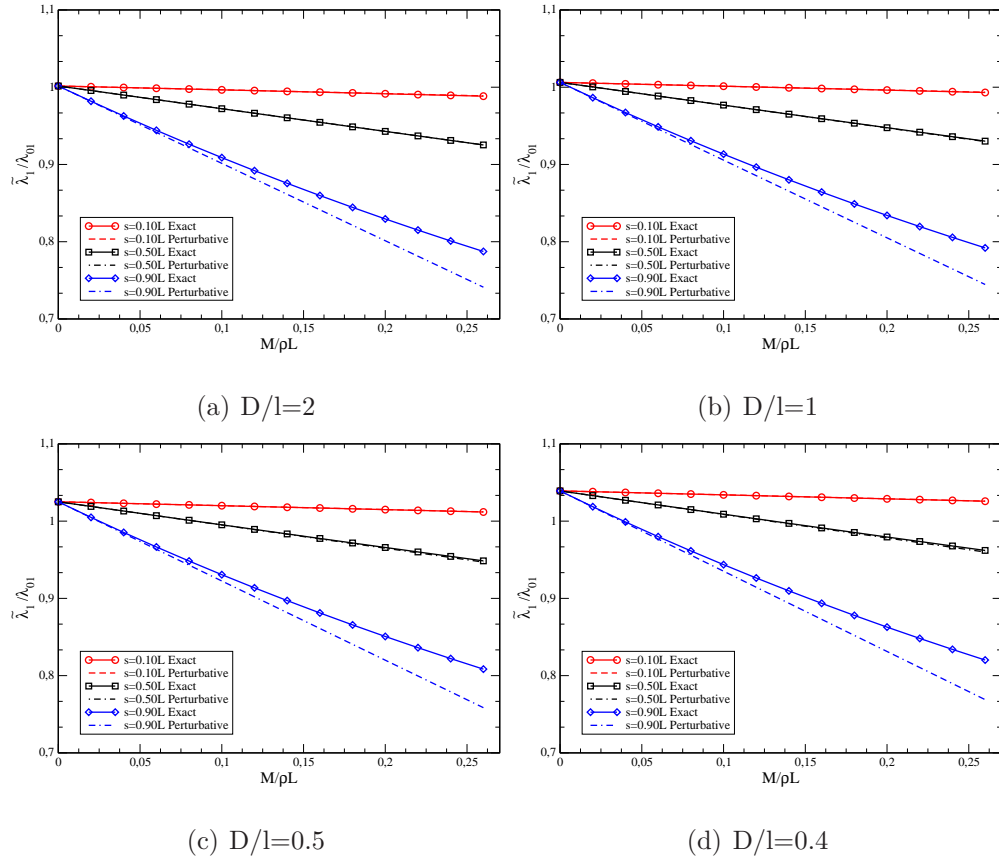


Figure 5: Clamped-free nanorod. Normalized first eigenvalue versus dimensionless point-mass, for different mass positions, and different values of the length scale parameter.

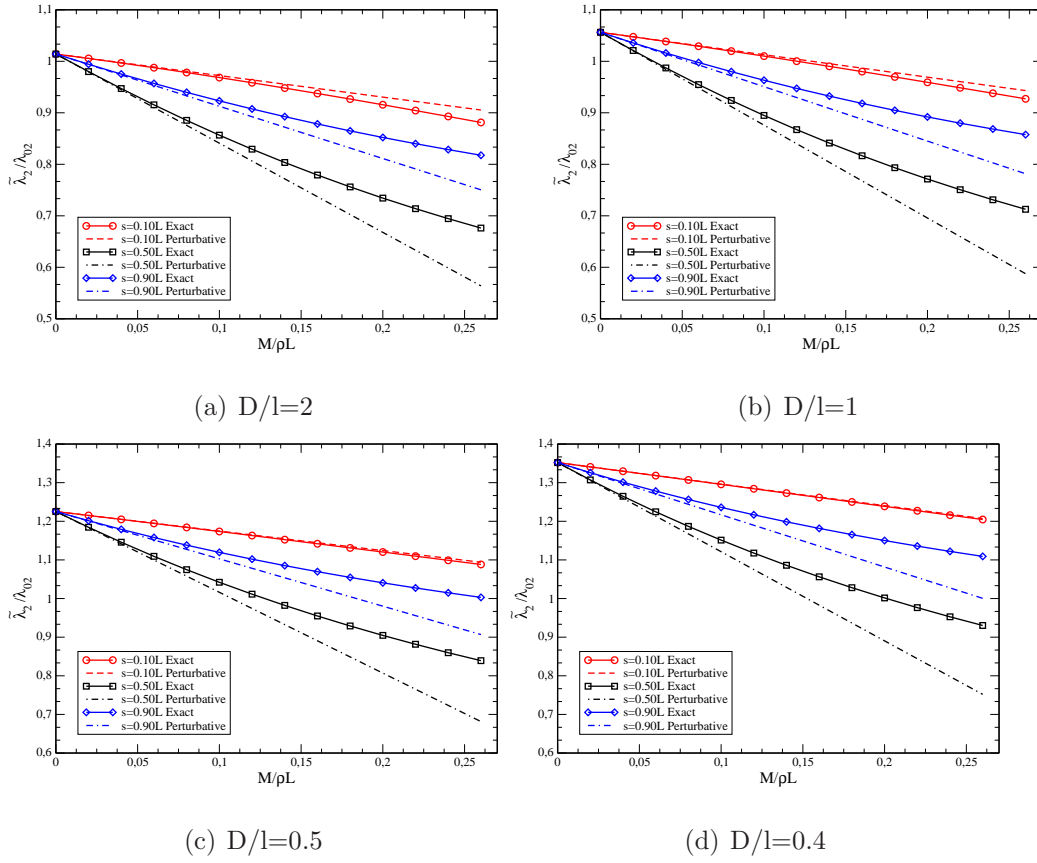


Figure 6: Clamped-free nanorod. Normalized second eigenvalue versus dimensionless point-mass, for different mass positions, and different values of the length scale parameter.

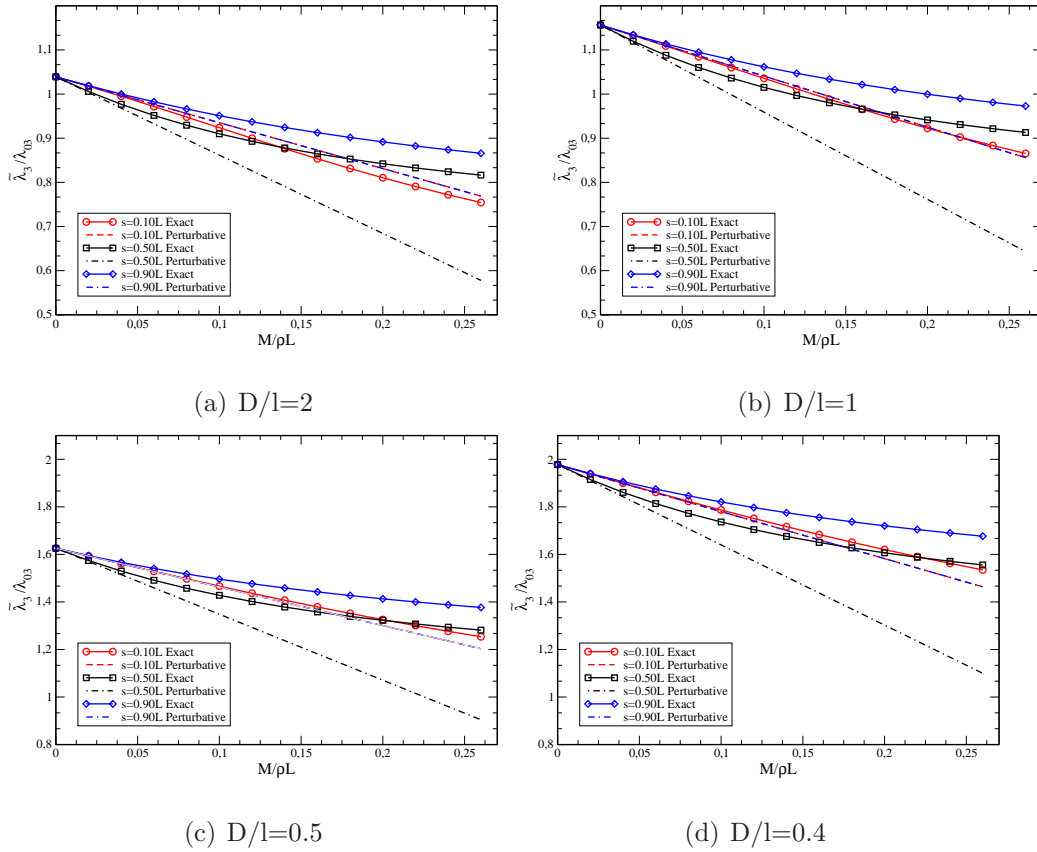


Figure 7: Clamped-free nanorod. Normalized third eigenvalue versus dimensionless point-mass, for different mass positions, and different values of the length scale parameter.